Diffusion in Nanoporous Materials: Challenges, Surprises and Tasks of the Day

Christian Chmelik,[1,2] *Seungtaik Hwang,*[1] *Jörg Kärger*[1,2]

[1] Faculty of Physics and Earth Sciences, Leipzig University, Linnéstraße 5, 04103 Leipzig, Germany

[2] Saxon Academy of Sciences and Humanities in Leipzig, Structural Commission "Propagation in Nature, Technology and Society", Karl-Tauchnitz-Straße 1, 04107 Leipzig, Germany

Corresponding author: Jörg Kärger; e-mail: kaerger@physik.uni-leipzig.de

Abstract

Diffusion is an omnipresent, most fundamental phenomenon in nature and thus critical for the performance of numerous technologies. This is in particular true for nanoporous materials with manifold applications for matter upgrading by separation, purification and conversion. The path lengths of molecular transportation within the industrial plants range from the elementary steps of diffusion within the micropores of the individual particles up to the matter flow over macroscopic distances. Each of them might be decisive in determining overall performance so that detailed knowledge of all modes of mass transfer is crucial for a knowledge-based optimization of the devices with reference to their transport properties. The rate of mass transfer is particularly complicated to be assessed within the individual (adsorbent) particles/crystallites with pore sizes of the order of molecular dimensions. We are going to present two powerful techniques exactly for this application, operating under both equilibrium (Pulsed Field Gradient (PFG) NMR) and non-equilibrium (Microimaging by interference microscopy and IR microscopy) conditions. The potentials of these techniques are demonstrated in a few showcases, notably including the options of transport enhancement in pore hierarchies. The contribution concludes with a survey on present activities within an IUPAC initiative aiming at the elaboration of "guidelines for measurements and reporting of diffusion properties of chemical compounds in nanoporous materials"

Keywords

Diffusion, Zeolites, Pore Hierarchies, Pulsed Field Gradient (PFG) NMR, Microimaging

1. Introduction

Nanoporous materials [1]–[3] are in the heart of numerous technologies of matter upgrading, including separation and chemical conversion. This is in particular true with zeolites [4]. Zeolites are distinguished by their regular pore structure, with diameters in the range of molecular sizes. The annual benefit that is attained worldwide by their exploitation in only petroleum refining has been estimated to at least 10 billion US dollars [5]. The excellent utility properties provided by nanoporous materials are a consequence of the intimate contact of their internal surface with the "guest molecules", giving rise to matter upgrading with a minimum of energy consumption and pollutant emission. Zeolites were thus, in the second half of the last century, among the first to foster "Non-Waste Technology and Production" and/or "Pollution Prevention", as a predecessor and promoter of today's "Green Chemistry" [6].

The performance of the technological application of nanoporous materials is easily understood to decisively depend on the intrinsic rate of mass transfer. This is a consequence of the fact that the gain in value-added molecules can never be faster than allowed by the rate of mass exchange between the material interior, i.e. the location of matter upgrading, and the surrounding. Diffusion, i.e. the random walk of the guest molecules accommodated in the nanoporous materials, is thus seen to become crucial for their technological performance, as it is already well known from many other materials, including solids with their manifold technological applications [7]–[9].

Differing from mass transfer in solids, where one is concerned with the migration of the constituents of the solid, i.e. of atoms or ions, diffusion studies in nanoporous materials mainly deal with the migration of guest molecules. Diffusion properties are thus a function of both the (nanoporous) solid (the "host" material) and the "guest" molecules. Moreover, one has to keep in mind that the rate of molecular propagation may become a function of the distances over which one is going to trace the diffusion paths. Section 2 provides a detailed discussion of the resulting different conditions under which diffusion measurement in nanoporous materials may be performed.

Over many years, the measurement of the rate of migration in the interior of the individual nanoporous particles/crystallites has proven to be a particularly challenging task. We are going to introduce two techniques, by which this type of measurement has become possible, one of them operating under equilibrium (Section 3) and the other under non-equilibrium (Section 4) conditions.

While the intimate contact between the guest molecules and the internal surface of the nanoporous host is a prerequisite of their technological performance in separation and conversion, it gives rise to a dramatic reduction of the diffusion rate and, hence, an impediment in the performance of the intended application. Section 5 illustrates how this conflict may be overcome by the use of materials with hierarchically organized pore spaces. The increasing complexity of the pore structure in such materials, however, notably complicates a quantitation of intrinsic mass transfer. Theoretical approaches and various options of experimental measurement for meeting these requirements are also presented. An inventory of existing measurement techniques and a consideration of the prerequisites for their successful interaction conclude the present article in Section 6.

2. The Various Regimes of Mass Transfer in Nanoporous Materials

Fig. 1 shows, in a cartoon-like manner, the spatial dimensions of relevance in an industrial plant, where nanoporous materials are typically used. The distances covered by the molecules on the way towards their upgrading are seen to range from nanometers, i.e. from the elementary steps of mass transfer in the micropores, up to the macroscopic dimensions of the plant. Displacements over each of these dimensions may, in principle, affect the overall rate of the output of value-added products. Detailed knowledge of the rate of mass transfer over these various dimensions is thus among the main prerequisites for a knowledge-based optimization of mass transfer in these devices.

Attainment of this information becomes progressively complicated with the decrease of the path lengths, over which mass transfer is to be traced, especially in the measurement of molecular diffusion in the interior of the individual crystallites/particles (bottom of Fig. 1). We are going to refer to it as "intracrystalline" diffusion. It is this process, which is in the focus of this paper.

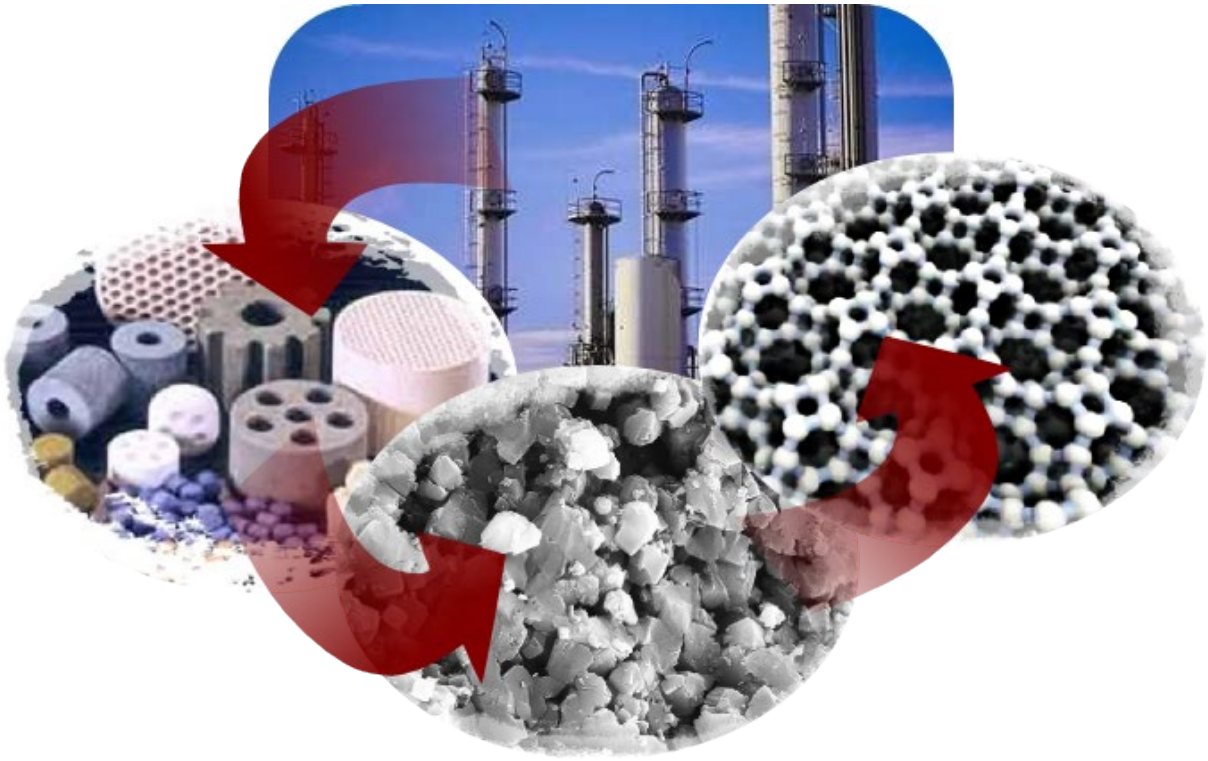

Figure 1: Nanoporous materials (adsorbents) are in the very heart of numerous technologies for matter upgrading. Relevant space scales range from molecular dimensions (fractions of nanometers, matching the pore sizes as shown on the right), over the dimensions of the individual adsorbent particles/crystallites of typically micrometers (bottom) and pelletized compacts of typical centimeters (left), up to the macroscopic dimensions of the plants (top).

An overview of the different situations, under which one is able to record intracrystalline diffusion, is provided in Fig. 2.

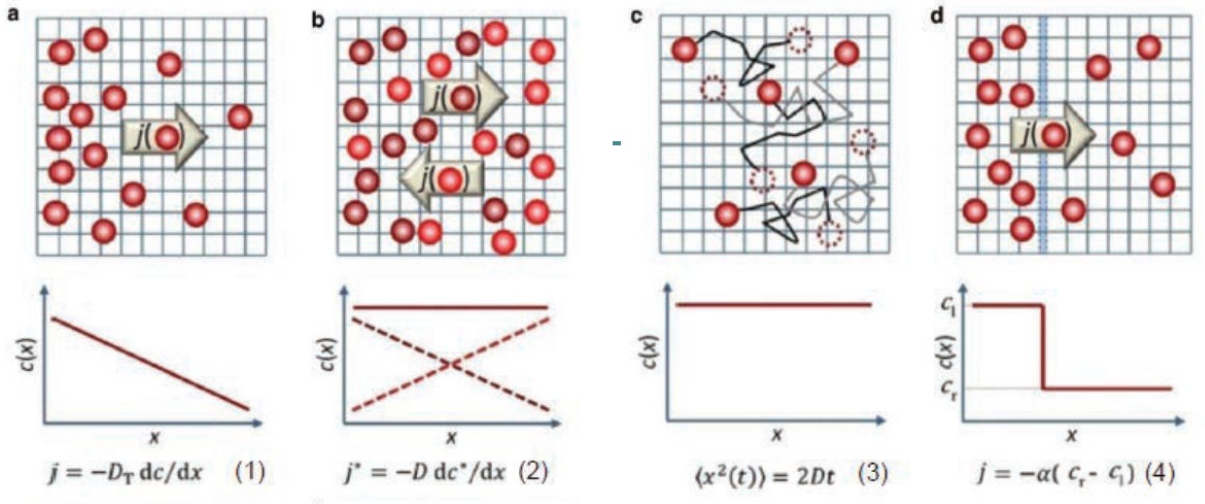

Figure 2: Different arrangements for the measurement of intracrystalline diffusion: (a) Non-equilibrium conditions, yielding the *transport* diffusivity via Fick's 1st law (eq. (1)). (b) Tracer exchange, simulating equilibrium conditions, yielding the *self-* (or *tracer*) diffusivity via Fick's 1st law (eq. (2)). (c) *Self-* (or *tracer*) diffusivity determined via the Einstein relation (eq. (3)) from the trajectory of the guest molecules under equilibrium. (d) Transport resistance acting in addition to the diffusional resistance within a crystal/particle or on its external surface and its quantitation via eq. (4) with the barrier permeability (or permeance) α, after [10].

Fig. 2a represents the most common situation, in which the flux density of guest molecules is recorded as a function of the gradient of the guest concentration. The factor of proportionality D_T in eq. (1) (Fick's 1st law) is referred to as the coefficient of *transport* diffusion (the "transport diffusivity"), indicating that we are indeed dealing with molecular transport. Alternatively and totally equivalently, also the terms chemical or collective diffusivities are in use. Conceptually, this type of mass transfer could also be described as an exchange between molecules (left in excess) with "holes" (right in excess).

It is the exchange of guest molecules with their labelled counterparts rather than with holes, which is considered in Fig. 2b. Labelled and unlabeled molecules may be distinguished from each other by the use of, e.g., different isotopes (as indicated by different shadings in the figure), but are otherwise assumed to be, notably in their microdynamic properties, identical. Now, the factor of proportionality appearing in Fick's 1st law (eq. (2)) is referred to as the self- or tracer diffusivity. As a consequence of the differences in the microphysical conditions as appearing from Fig. 2, the coefficients of self- and transport diffusion are immediately seen to be, as a rule, different from each other. They must only be expected to coincide in the limit of sufficiently small guest concentrations when the mutual interaction of the molecules may be assumed to be negligibly small in comparison with their interaction with the internal host surface. This may be understood as an immediate consequence of the fact that, in the limiting case of missing mutual interaction, it makes no sense anymore to distinguish between non-equilibrium (Fig. 2a) and equilibrium (Fig. 2b) conditions [11]

With the notation of the concentrations and fluxes in eqs. (1) and (2) and their application to the situation shown in Fig. 2, the extensions of the elementary volumes and areas to which they are related, are implied to be notably larger than the pore dimensions, but sufficiently small in comparison with the particle/crystallite extension. With, typically, pore sizes of nanometers and particle/crystallite sizes of micrometers, this requirement may generally be assumed to be fulfilled [12].

Fig. 2c shows the trajectories of five guest molecules over a fixed time interval. This is the situation typically encountered in diffusion measurement by the pulsed field gradient (PFG) technique of NMR [3],[13],[14], quasi-elastic neutron scattering (QENS [3],[15]–[17]) and single-particle tracking (SPT [18],[19]). These techniques are able to provide information about typical diffusion path lengths and thus, via Einstein's diffusion equation, eq. (3), about the intracrystalline self-diffusivities. As a prerequisite, the diffusion path lengths must be required to be sufficiently large in comparison with the pore sizes and sufficiently small in comparison with the particle/crystal extensions. Detection of the equivalency of eqs. (2) and (3) for the determination of self-diffusivities was among Einstein's great discoveries in his "annus mirabilis" 1905 [20],[21].

It is worthwhile mentioning that, in eq. (3), it is not specified whether the average as required on the left-hand side is to be taken over all molecules over an identical time interval or over one and the same molecule over subsequent time intervals. Equivalence between these two types of averaging under equilibrium conditions is the main message of the ergodic theorem of statistical physics [22]. Combining the information of diffusion measurement by PFG NMR and SPT, ref. [23] provides a first experimental proof of the validity of this theorem for the diffusion of guest molecules in nanoporous host materials.

Fig. 2d, finally, takes into account that deviations from the regular structure of the adsorbent particles (by, e.g., stacking faults [24]) may give rise to internal transport resistances acting in addition to the diffusion resistance by the genuine pore system. These resistances may be quantitated by a relation of the type of eq. (4). The permeability (or permeance) α is defined as the factor of proportionality between the flux through this resistance and the difference in guest concentration between each side. Such resistances are particularly likely to occur on the outer surface of the adsorbent particles/crystals. In this case, on the right-hand side of eq. (4), one has to consider the difference between the intracrystalline concentration $c_{\mathrm{eq.}}$ that would be established in equilibrium with the external gas (or fluid) phase and the intracrystalline concentration c_0 in the vicinity of the external surface, yielding

$$j = -\alpha\left(c_{\mathrm{eq.}} - c_0\right). \tag{5}$$

The subsequent sections are dedicated to two experimental techniques applied for investigating intracrystalline diffusion under equilibrium and non-equilibrium conditions.

3. Diffusion Measurement by the NMR Pulsed Field Gradient (PFG) Technique

For rationalizing the principle of diffusion measurement by PFG NMR (a more stringent introduction may be found in, e.g., refs. [13],[25]–[27]) it is sufficient to confine oneself to the quasi-classical conception of nuclear magnetism by assuming that a nuclear spin combines the properties of a gyroscope and a magnetic dipole, thus disposing of a mechanical and magnetic moment. Therefore, similarly as a mechanic gyroscope under the influence of gravity, also a nuclear spin (notably a proton as the nucleus of hydrogen) rotates ("precedes") about the direction of a constant magnetic field. The frequency of this rotation (top right in Fig. 3) may be determined to be

$$\omega = \gamma B \qquad (6)$$

with B denoting the intensity of the magnetic field. The factor γ is a characteristic quantity of the nucleus under study, the "gyromagnetic ratio", which results from the ratio between the mechanical and magnetic moments.

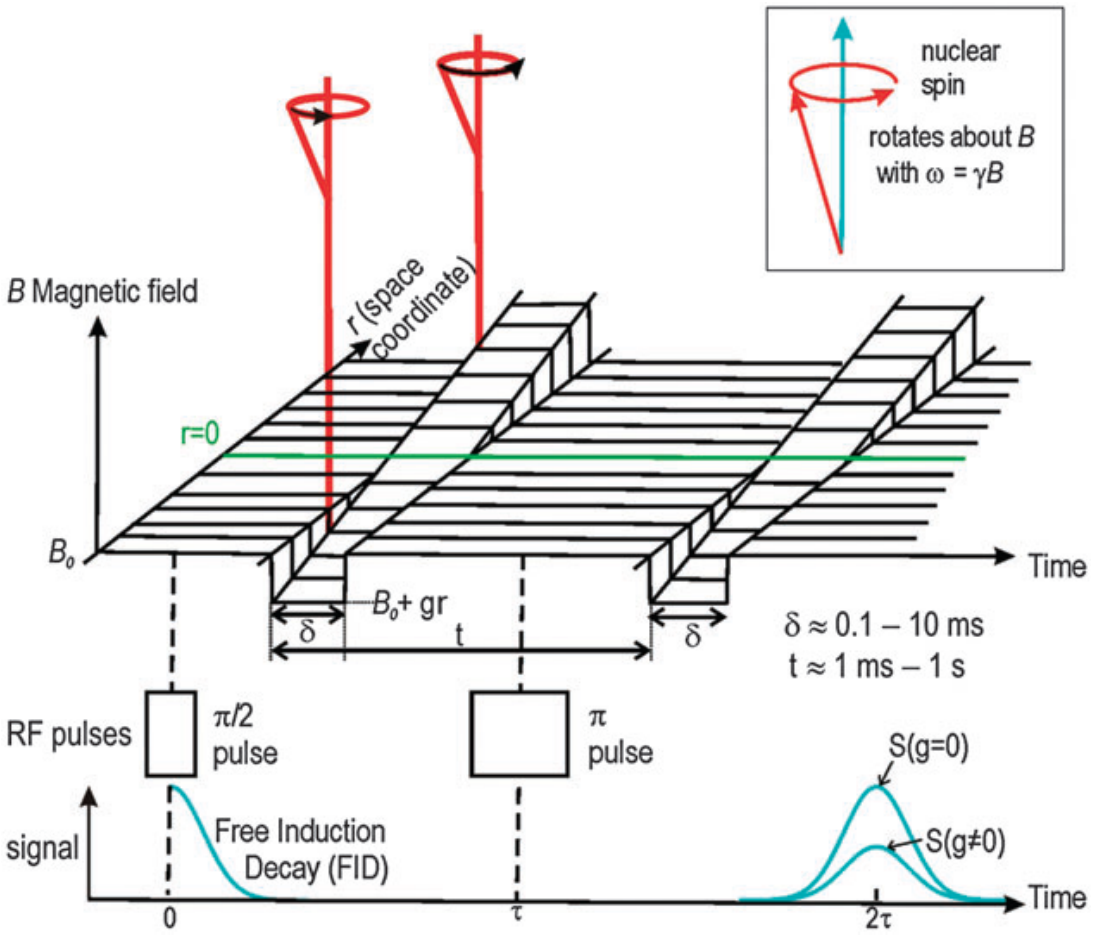

Figure 3: Schematics of diffusion measurement by PFG NMR: A sequence of radio-frequency (RF) pulses gives rise to the formation of a signal. The intensity S of this signal becomes, under the influence of a pair of field gradient pulses (i.e. a strongly inhomogeneous magnetic field superimposed on the constant magnetic field commonly used in NMR), a function of the diffusion properties of the molecules that contribute to the observed signal. Reproduced from Ref [28], copyright 2015, with permission from John Wiley and Sons.

With a suitably chosen RF pulse ("$\pi/2$ pulse"), the magnetic moments of the individual spins may be aligned into a direction perpendicular to the constant magnetic field, giving rise to a rotating magnetization. This rotating magnetization induces in a suitably arranged (receiver) coil a voltage, which is recorded as the NMR signal.

In Fig. 3 the constant magnetic field B_0 is seen to be superimposed, over two short time intervals δ, by two strongly inhomogeneous fields gz (where the space coordinate $\mathbf{r}$ is imposed to show in z direction). Now, during the field gradients, the rotational frequency of the spins becomes a function of the location so that the vector sum of the individual magnetizations drops to zero. With the application of a second, identical field gradient pulse and a, once again suitably

chosen, RF pulse (a "π pulse"), the effect of spreading of the first field gradient pulse is counterbalanced. This compensation, however, does only operate if, during the two field gradient pulses, each individual spin experiences the identical strength of the magnetic field. Any difference Δz in the positions of a spin during the first and second field gradient pulse, obviously, gives rise to a deviation

$$\Delta\varphi = \delta\Delta\omega = \delta\gamma g\Delta z \tag{7}$$

of the direction of the magnetic moment of this particular spin from the mean direction. Such spins do only contribute with the cosine of this angle to the overall magnetization. Signal attenuation due to molecular displacements within the sample under the influence of field gradients may therefore be noted as

$$\psi(g\delta, t) = \frac{S(g)}{S(g=0)} = \int_{-\infty}^{\infty} P(z,t)\cos(\delta\gamma gz)dz. \tag{8}$$

$P(z,t)$ stands for the probability (density) that during time *t*, i.e. within the interval between the two field gradient pulses, an arbitrarily selected molecule is shifted over a distance *z* (i.e. in the direction of the pulsed field gradient). It is referred to as the "mean propagator" [29],[30] and, with eq. (8), seen to result from the inverse Fourier transform of the PFG NMR signal attenuation $\psi(g\delta, t)$.

For normal diffusion in a homogenous space, the propagator is known to be given by a simple Gaussian [3],[7]–[9]

$$P(z,t) = (4\pi Dt)^{-1/2}\exp\left(-\frac{z^2}{4Dt}\right), \tag{9}$$

with *D* denoting the self-diffusivity. Inserting eq. (9) into (8) yields the key formula for diffusion measurement by PFG NMR

$$\psi(g\delta, t) = \exp(-\gamma^2 g^2\delta^2 Dt) = \exp\left(-\frac{1}{2}\gamma^2 g^2\delta^2\langle z\rangle^2\right), \tag{10}$$

with the second equality resulting from the Einstein relation, eq. (3), correlating the diffusivity with the observation time and the molecular mean square displacement in the gradient direction.

Alternatively and completely equivalently, PFG NMR is as well referred to as pulsed gradient spin echo (PGSE) NMR and NMR diffusometry.

An overview of the wealth of information on diffusive mass transfer in beds of nanoporous crystals as provided by this technique is given by Fig. 4. Plotted are (due to symmetry reasons only one half of) the mean propagators $P(z,\Delta)$ of the guest molecules for different observation times. A short summary of the thus attainable information is given in the following, for a more detailed introduction we refer to Section 11.4 in the textbook, ref. [3].

In the situation shown top left, the diffusion path lengths are notably smaller than the crystal extension. Under these conditions, as a consequence, one is recording (by plotting the signal attenuation vs. the gradient intensity via eq. (10)) the intracrystalline diffusivity.

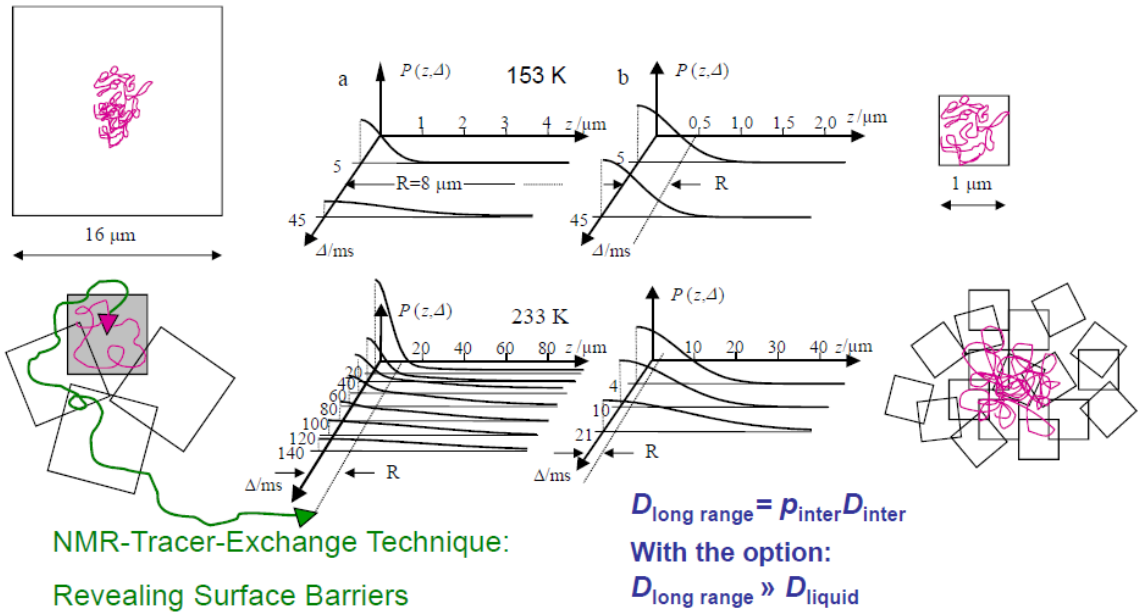

Figure 4: Classical showcase illustrating the evidence provided by PFG NMR on investigating diffusion in a bed of nanoporous crystals (ethane in zeolite NaCaA with two different crystal sizes) over different diffusion path lengths: mean propagators $P(z,\Delta)$ plotted for different observation times $\Delta \equiv t$ (= distance between the gradient pulses). Time and space scales are typically in the range of milliseconds and micrometers, as in the given example. Reproduced from [31] with permission from the Royal Society of Chemistry.

Under the conditions considered in the presentations top right, molecules encountering, from the crystal interior, the external surface of the crystal are found to be, essentially, reflected to the interior. Now, in the limit of sufficiently large times, PFG NMR signal attenuation is found to be determined by the size of the crystal rather than by the intracrystalline diffusivity, with the diffusivity appearing in eq. (10) becoming an only "apparent" diffusivity which, for spherical particles of radius R, obeys the relation [3]

$$D_{restr.} = \frac{R^2}{5t} \quad . \tag{11}$$

With increasing temperature (bottom right), the relative amount of molecules in the intercrystalline space is increasing. More and more molecules are then able to leave the crystals on encountering their outer surface. Now, as a good approximation, the effective diffusivity as attainable by PFG NMR (with root mean square displacements notably exceeding the crystal sizes) may be noted as

$$D_{\mathrm{long-range}} = p_{\mathrm{inter}} D_{\mathrm{inter}} \tag{12}$$

with p_{inter} ($\ll 1$) denoting the relative amount of guest molecules in the intercrystalline space and D_{inter} their diffusivity. It is worthwhile noting that $D_{\mathrm{long-range}}$, given the high mobility in the intercrystalline space, may even notably exceed the diffusivity in the pure liquid [32]–[34].

The information provided by PFG NMR is even further increased if – by the use of sufficiently large crystals and a corresponding spatial resolution – the rate of molecular propagation may be recorded both in the interior of the crystals and through the intercrystalline space (bottom left). Then, in addition to the measurement of intracrystalline diffusion, one is as well able to

determine the relative amount of molecules which, after the given observation time, have left their crystals. The thus attainable information corresponds with that of a conventional tracer exchange experiment. In view of the short exchange times accessible by NMR, it is also referred to as the fast tracer desorption technique [35],[36]. Under diffusion limitation, the mean exchange time (= the first statistical moment, see e.g. [37],[38] or section 13.6.2 in [3]) between a spherical particle of radius R and its surroundings obeys the relation

$$\tau_{\mathrm{Diff}} = R^2/(15D). \tag{13}$$

PFG NMR offers the possibility to directly determine the mean exchange time by recording NMR tracer exchange and to calculate, via eq. (13), the tracer exchange time under diffusion limitation. Mutual comparison provides direct evidence of the existence and intensity of transport resistances by surface barriers. It was one of the spectacular results of PFG NMR that in numerous technological applications molecular exchange and, hence, also uptake and release was found to be controlled by the formation of surface resistances rather than by intracrystalline diffusion [39]–[41]. Under barrier limitation, the mean exchange (uptake or release) time becomes ([37] or section 13.6.2 in [3])

$$\tau_{\mathrm{Barr}} = R/(3\alpha). \tag{14}$$

Eqs. (13) and (14) provide a reasonable estimate for also more complex particles if the parameter R is understood to denote the radius of a sphere whose surface-to-volume ratio (A/V) coincides with that of the particle under study, yielding

$$R \equiv 3V/A. \tag{15}$$

4. Diffusion Measurement by Microimaging

Fig. 5 provides a short introduction to the measuring principles of interference microscopy (IFM) and IR Fourier transform spectroscopy (IRM) for the recording of transient concentration profiles during uptake and release of guest molecules by nanoporous materials, following ref. [42]. For more detailed information we refer to section 12.2 in [3] quite in general and to [43],[44] for IFM and [45],[46] for IRM. Spatial resolution may attain fractions of micrometers by IFM and is typically in the order of a few micrometers for IRM. Information about concentrations is provided in relative units. Absolute values become accessible by comparison with the result of conventional gravimetric measurement of the amount adsorbed as a function of the pressure externally applied.

Both techniques yield the integral of the local concentration in observation direction over the crystal/particle under study. With pore spaces extended in one or two dimensions and observation perpendicular to them, information provided by the integral coincides with the local concentration. This is the case with even 3d pore spaces on considering crystals/particles in the shape of platelets, with the top and bottom faces sealed (but permeable for light!), so that mass transfer during adsorption and desorption is anyway confined to the direction perpendicular to the direction of observation.

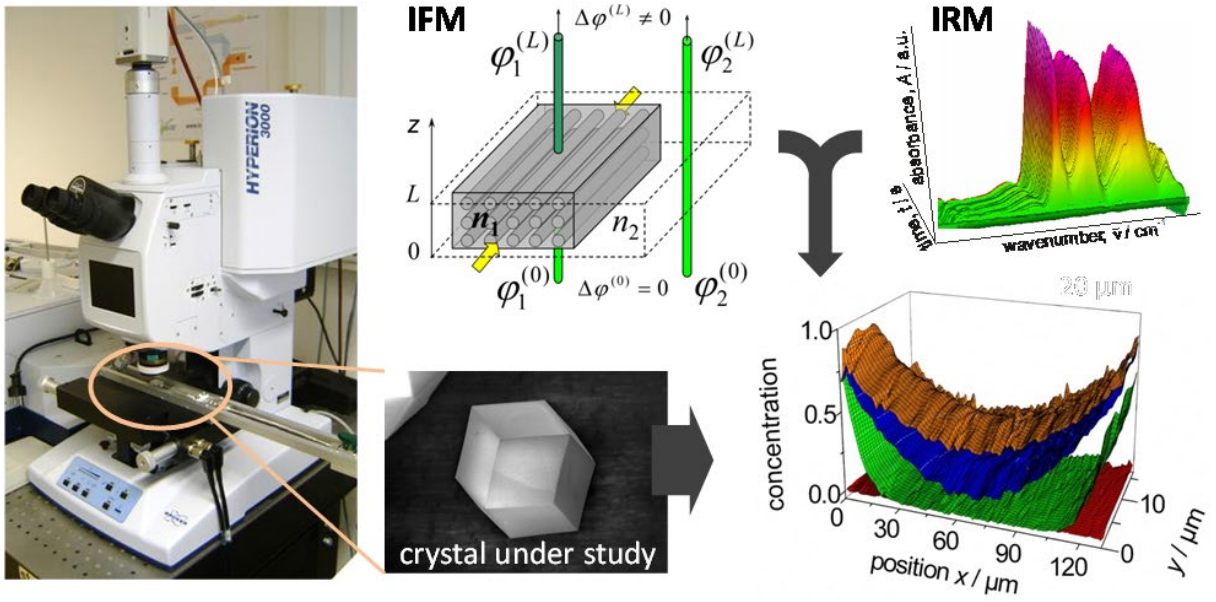

Figure 5: Fundamentals of Microimaging. The crystal under study (bottom center) is positioned under a microscope (left). Information about the intracrystalline concentration (more correctly: the concentration integral in observation direction) is attained in interference microscopy (IFM) by an analysis of the phase shift between a light beam passing the crystal and a standard (top center) and in Fourier transform IR spectroscopy (IRM) from the signal intensity recorded by an array of IR detectors in the focal plane (top right). In either case, the resulting information may be plotted as a 2d-representation of the evolution of the concentration integral in observation direction during, e.g., adsorption at subsequent instants of time (bottom right). Reproduced from [42] with permission from Springer Nature.

Microimaging by interference microscopy (IFM) and by IR microscopy (IRM) are able to provide us with guest profiles in nanoporous materials which, so far, were mainly known from the representations in the textbooks by Crank [47] and Carslaw & Jaeger [48]. An example is provided by Fig. 6 [49]–[51]. It shows, with the four upper representations, the evolution of the guest profiles during adsorption (left) and desorption (right), stimulated with a small pressure step (top) and a large pressure step (middle).

During the small pressure step, guest concentration and, hence, the guest diffusivity, may be implied to remain constant. Fick's 2nd law simplifies, therefore, to a linear differential equation, with the sum of two solutions (for, e.g., uptake and release) being as well a solution (e.g. constancy in space and time in the considered case). This exactly is the situation observed for tracer exchange, where the concentrations of the two components (labelled and unlabeled molecules) anywhere within the sample add up to constancy. This constancy does, essentially, appear in the lower left presentation (Fig. 6e). By a corresponding choice of the ordinate notation, it provides a comparison between the relative amount of guest molecules which *during desorption have not yet left the crystal* and which *during adsorption are still to enter*. Both agree, just as it is obviously the case during tracer exchange.

This is not anymore the case on looking at the large pressure step and the resulting concentration change, for which the concentration may be determined to increase by one order of magnitude [49]–[51]. With the diffusivity becoming a function of the concentration, Fick's 2nd law loses the favorable properties offered by a linear equation. Adsorption and desorption profiles are now by far not compatible anymore. In fact, molecular uptake is by about one order of

magnitude faster, which nicely corroborates with the corresponding increase in the diffusivity. Molecular desorption, on the other hand, is most impressively found to proceed at a similar rate as both ad- and desorption at the small concentration (Fig. 6f).

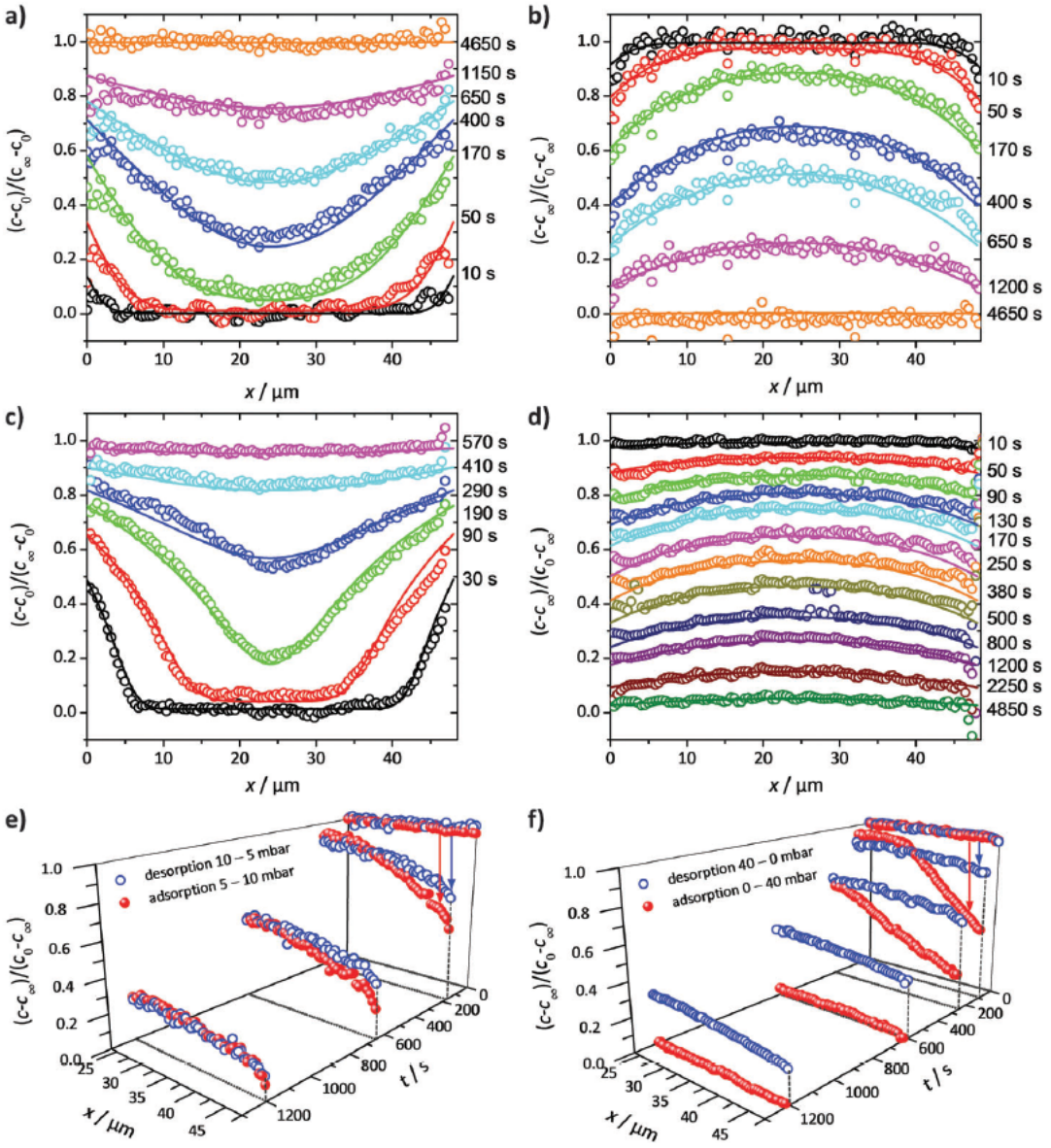

Figure 6: Transient concentration profiles during uptake (a, c) and release (b, d) of methanol in ferrierite-type zeolites along the 8-ring channels at room temperature induced by a pressure step between 5 and 10 mbar (a, b) and 0 and 40 mbar (c, d) in the surrounding atmosphere. By plotting the concentrations from top to bottom for adsorption, in plots (e) and (f) profiles after selected times during ad- and desorption are shown in a unified representation (with, due to symmetry, only one half shown). Reproduced from [50] with permission from the Centre National de la Recherche Scientifique (CNRS) and the Royal Society of Chemistry.

Quantitation of surface barriers by PFG NMR is based on a comparison between the tracer exchange time as attainable by the NMR tracer desorption technique and its estimate via eq. (13). In general, both values are accessible with only significant uncertainty. As a consequence, absolute values of surface permeabilities may only be determined with an appreciable accuracy

(of, say, a factor of 2 or better) if their influence notably exceeds the transport resistance by intracrystalline diffusion. This limitation does not exist anymore for microimaging where, via eq. (5), surface permeability become accessible, as soon as the boundary concentration during transient uptake is observed to be markedly smaller than the boundary concentration finally attained under equilibrium. This is the situation as quite generally seen in Fig. 6.

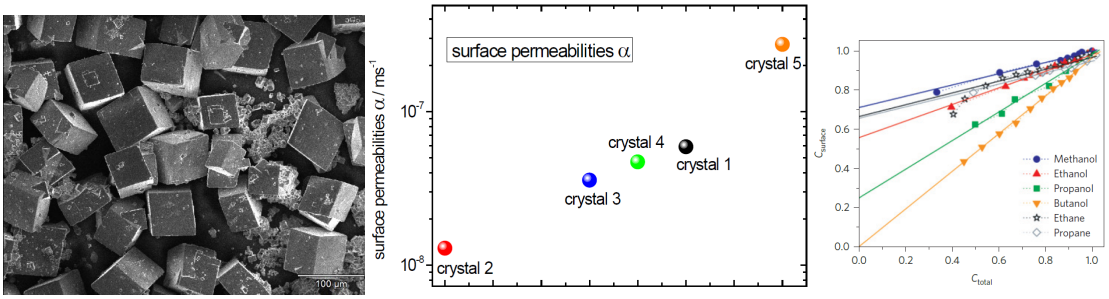

(a) (b) (c)

Figure 7: Surface barriers on zeolite SAPO-34. Irrespective of the structural similarity of the individual crystals of zeolite SAPQ-34 as appearing from their SEM picture (a), their surface permeabilities as probed with methanol by IFM are found to vary over more than an order of magnitude (b). By plotting the boundary concentration as a function of overall uptake ("Heinke-Kärger plots", (c)) the contribution of the surface resistance to the overall resistance of uptake or release (i.e. the combined influence of surface and diffusion resistance) as resulting from the ordinate intercept of the long-time asymptote of c_{surf}/c_0 vs. m_t/m_∞ (see eq. (16)) is seen to depend on the nature of the molecule under study. Reproduced from [52] with permission from Springer Nature.

Fig. 7 presents the results of a detailed study of the surface resistances as observed with zeolites of type SAPO-34 as a key material for important technological applications including the methanol-to-olefin (MTO) process [53] and propane-propene separation [54]. With methanol as a probe molecule, the surface permeabilities of different crystals are found to vary over more than an order of magnitude (Fig. 7a), irrespective of the similarity in the appearance of the crystals as seen in Fig. 7b.

The information as provided by microimaging allows the representation of the (normalized) boundary concentration c_{surf}/c_0 as a function of the relative total uptake m_t/m_∞ at any instant of time. Such plots are displayed in Fig. 7c for one and the same crystal and various guest molecules. Of particular significance is the ordinate intercept w of the long-time asymptote of c_{surf}/c_0 vs. m_t/m_∞. It provides, via the relation

$$w^{-1} \approx \frac{\tau_{\mathrm{Diff}}+\tau_{\mathrm{Barr}}}{\tau_{\mathrm{Diff}}}, \qquad (16)$$

an estimate of the enhancement of the exchange (uptake or release) time due to the influence of the surface barrier. The significance of this estimate is easily rationalized in the two limiting cases:

Under limitation by exclusively the surface barriers, guest concentration during e.g. uptake increases uniformly over the whole crystal. This means that c_{surf}/c_0 increases linearly with m_t/m_∞, yielding an ordinate intercept of $w = 0$. Thus, by Eq. (16), the increase in the mean

exchange time is infinite, which means that the transport limitation is actually caused by exclusively the existence of the surface barrier.

For negligible surface resistances, boundary concentration will immediately assume the equilibrium concentration, yielding $c_{\mathrm{surf}}/c_0 = 1$ starting with the very beginning of molecular uptake, i.e. with $m_t/m_\infty = 0$. The ordinate intercept is thus found to be equal to $w = 1$. As to be required, surface barriers are thus, via eq. (16), seen to be without any influence.

Representations as displayed in Fig. 7c ("Heinke-Kärger plots", following refs. [52],[55],[56]) may help in clarifying the origin of the surface barrier, i.e., in particular, to decide whether the resistance is caused by a significant, essentially homogenous reduction of the permeability all over the crystal surface or by a total blockage of a major part of the external crystal surface with a few "holes" allowing an essentially unimpeded passage of the guest molecules. Assuming holes of radius r in a square-lattice arrangement of mutual distance L ($\gg r$), in the latter case, e. g., an effective medium approach yields

$$\alpha = \frac{2Dr}{L^2}, \tag{17}$$

with the intracrystalline diffusivity appearing as a factor of proportionality [57],[58]. Both the transport resistances due to intracrystalline diffusion (eq. (13)) and surface permeation (eqs. (14, 17)) are thus seen to be inversely proportional to the intracrystalline diffusivity. The ratio between these two resistances, as appearing in the ordinate intercept w of the long-time asymptote of c_{surf}/c_0 vs. m_t/m_∞ would therefore be expected to be independent of the intracrystalline diffusivity and, hence, of the molecule under study. For the system considered in Fig. 7c this is obviously not the case. Surface barriers built up in the SAPO-34 samples under study have to be associated therefore with the formation of an essentially homogeneous layer of reduced permeability covering the whole crystal surface.

With the evidence of PFG NMR and microimaging, the occurrence of transport resistances on the outer surface of the individual particles and crystallites is today generally accepted to affect, in numerous cases, overall mass transfer to an extent comparable with or even exceeding intracrystalline diffusion [59]. So far, there is, obviously, no general rule about the nature of these resistances. While in the studies presented with Fig. 7 surface barriers have been recognized as a layer of significantly reduced permeability, similarly as already implied in the early PFG NMR studies for revealing the origin of the deterioration of zeolites during their use for catalytic conversion and/or mass separation in industrial plants [40],[60],[61], for other systems there exists well-founded evidence that surface barriers are caused by a total blockage of the external surface, with the exception of a few "holes" scattered over the surface, giving rise to a permeability following eq. (17) [62],[63]. In such a case, e.g., among more than a thousand of "windows" connecting the intracrystalline space with the surroundings (see Fig. 1 on the far right) only one may be found to be permeable. The quantitation and specification of transport resistances at the interface between a nanoporous bulk phase and the surroundings is thus among the challenging tasks of current research with nanoporous materials, involving both the development of theoretical tools [64]–[68] and highly resolved experimental measurement of surface structure and composition [69]–[72].

5. Transport Enhancement in Pore Hierarchies

While the intimate contact between the internal surface of nanoporous materials and the guest molecules is an indispensable prerequisite of their functionality under industrial use, e.g., for

matter separation and conversion, it sets an upper limit on the molecular mobility and, hence, on the rate at which the value-added product may be delivered from the origin of its production, the space of micropores. This limitation may be overcome in more complex systems with a network of larger ("transport") pores, permeating a microporous bulk phase. Among a large spectrum of possibilities to combine different types of pore spaces to pore hierarchies [73],[74], this possibility is distinguished by its most favorable transport properties and the option of being captured by an analytical approach, regardless of the given complexity. Since zeolites permeated by networks of mesopores (most recently by even macropores [75]) are the by far most important representatives of this class of materials [76]–[80], we are going to refer to them quite generally as mesoporous zeolites.

5.1 An Introduction via Kinetic Monte Carlo (KMC) Simulation

We use the potentials of conventional kinetic Monte Carlo (KMC) simulation [81]–[85] (see, also, Sect. 9.3 in [3]) to capture the main features of mass transfer in hierarchically organized pore spaces and follow, essentially, the presentation given in [86]. The simulation scheme is displayed in Fig. 8. A homogeneous microporous bulk phase (top right) is traversed by an array of mutually perpendicular channels in all three directions. They represent the space of the mesopores (rightmost in the figure). Diffusion is implied to proceed on a regular grid of equidistant sites (bottom left). The jump probabilities (to be associated with the energy profile given bottom right) are chosen to comply with both the different diffusivities in the mesopores (D_1) and micropores ($D_2 \ll D_1$) and occupation probabilities p_1 and p_2 ($= (1 - p_1) \gg p_1$). Here and in the following the indices 1 and 2 are used as a label for the meso- and micropores.

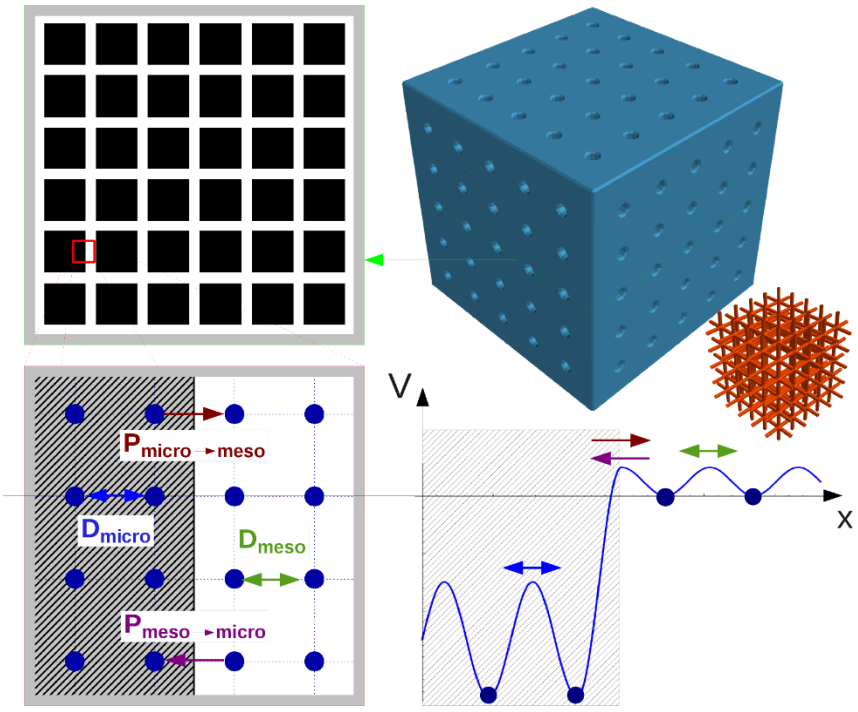

Figure 8: Investigating mass transfer in a pore hierarchy as typical for mesoporous zeolites by kinetic Monte Carlo (KMC) simulation. Reproduced from [86], copyright 2015, with permission from John Wiley and Sons.

Fig. 8 shows a simplified presentation of the simulation model with only $5 \times 5 \times 5$ channels while, in the simulations, $18 \times 18 \times 18$ channels have been considered. The cross-section of

the channels is built up by 2×2 lattice points. In between adjacent parallel channels are 8 lattice points. The model system does thus consist of altogether $190 \times 190 \times 190$ lattice points. The volume ratio of the two domains results to be $\frac{V_1}{V_2} = 0.111$.

In all simulations, the step in the potential energy at the micro-mesopore interface is taken into account by setting the jump rates $p_{2\to1}/p_{1\to2}$ =1/10. As a requirement of dynamic equilibrium, it holds therefore for the equilibrium concentration in the two pore spaces $\rho_2^{\mathrm{eq}} = 10\rho_1^{\mathrm{eq}}$. Combining these values with the respective volumes, the occupation probabilities of the two pore spaces under equilibrium conditions are thus found to be p_1= 0.0105 and p_2= 0.9895.

Molecular uptake from the surrounding atmosphere was simulated on an initially empty lattice. All outer lattice points were kept at a mean site occupation probability of 1/10, corresponding to the concentration in equilibrium with the surroundings. During a simulation step, all molecules on the grid of lattice points were allowed to jump at the rates corresponding to the given lattice points. Jumps are allowed to occur independently of whether or not the sites they are directed to are occupied, reflecting the situation of concentration independent diffusion.

Two examples of the thus evolving profiles of intracrystalline concentrations are shown in Fig. 9. Guest profiles are recorded at two subsequent instants of time, for loadings (relative guest densities) of, respectively, 0.2 and 0.7. The density profiles shown on the left have been obtained by evaluating a cylinder-shaped cut through the system center with a radius covering 15 lattice nodes (space between the two lines shown in the cross section on the right), with each value of $\rho(x)$ representing the average over the cross-section of the cylinder at position x. The presentations on the right-hand side show the guest distributions over a cross-section through the model system at the two instants of time when the profiles shown on the left have been recorded.

The examples differ in only the ratio between the meso- and micropore diffusivities, namely $D_1 = 10^2 D_2$ (top) and $D_1 = 2.5 \times 10^5 D_2$ (bottom). The particularly large ratio appears in a pronounced filling of the mesopores (as seen in the peaks bottom left) and an essentially homogeneous increase in loading all over the system (profiles bottom left and guest distribution bottom center and right). The space of mesopores, obviously, is filled long before an appreciable amount of molecules has entered the micropores. This situation is referred to as the limiting case of slow exchange.

Reduction in the ratio (i.e. enhancement of D_2 just as a reduction of D_1) leads to a striking change in distribution pattern (top of Fig. 9). Now, molecular uptake is seen to occur with a diffusion front, propagating essentially simultaneously through the space of micro- and mesopores. We are now in the limiting case of fast exchange, with a resulting ("effective") diffusivity given by the weighted mean of the diffusivities in the two pore spaces

$$D_{\mathrm{eff}} = p_1 D_1 + p_2 D_2. \qquad (18)$$

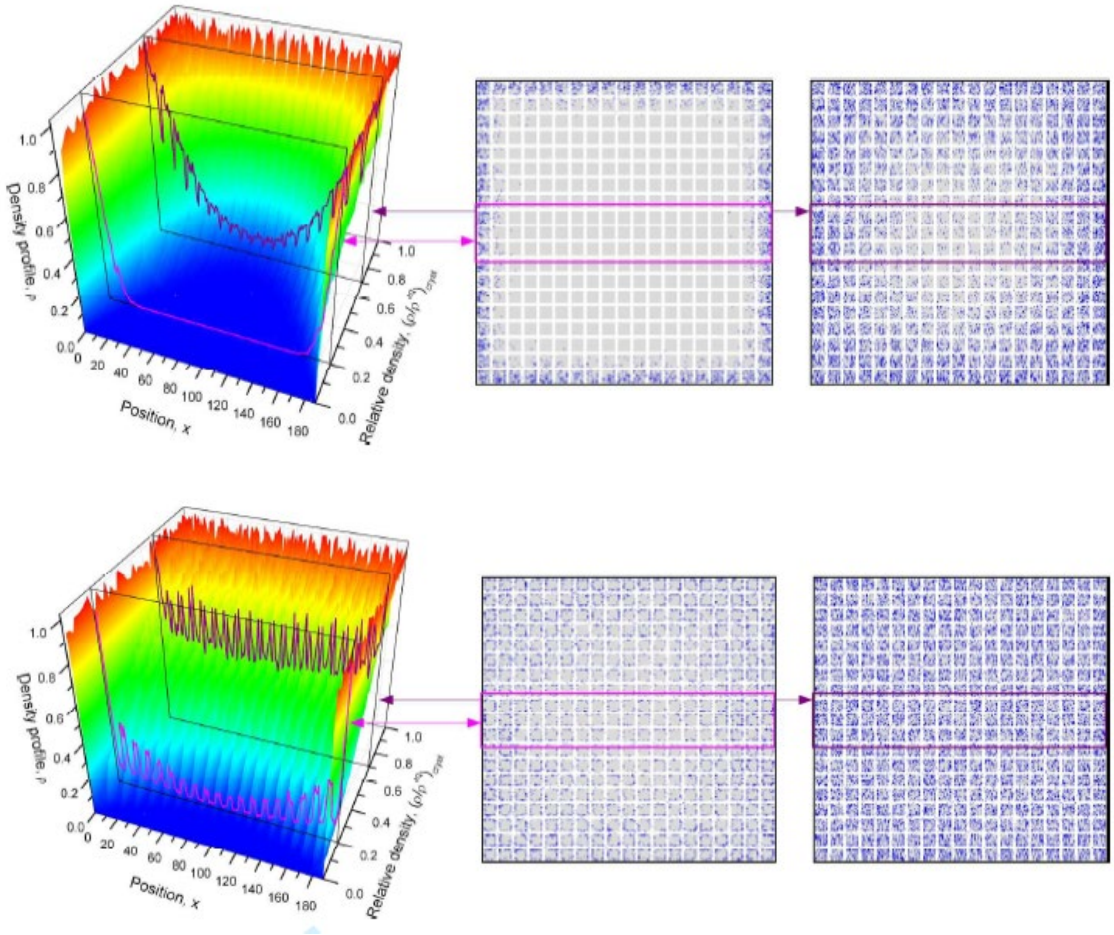

Figure 9: Representation of the concentration profile during molecular uptake in the model system shown in Fig. 8 when 20% (central column) and 70% (right column) of equilibrium loading have been attained. Representations on the left show, at these instants of time, the concentration profiles along a cylindrical channel with the contour as given by the violet lines on the right. Representations on the right show examples of the guest distribution over a cross-section through the system at these times. The diffusivity in the transport (meso-) pores (D_1) exceeds the diffusivity in the micropores (D_2) by a factor of 10^2 in the upper representation and of 2.5×10^5 in the lower one. Reproduced from [86], copyright 2015, with permission from John Wiley and Sons.

In view of the difference in the nature of the dominating mechanisms, also the time constant τ of molecular uptake (release or exchange) must be expected to be different. In fact, in the limiting case of fast exchange, overall mass transfer may be implied to be completely described with an effective diffusivity given by eq. (18). The time constants of uptake (release and exchange) are thus determined via eq. (13), yielding

$$\tau = \tau_{(\text{fast exch})} = \frac{R^2}{15(p_1 D_1 + p_2 D_2)}. \qquad (19)$$

In the limit of slow exchange, molecular uptake may be understood to occur via the interface between the (essentially instantaneously filled) mesopores and the bulk of micropores. Hence, for quantifying the time constant $\tau_{(\text{fast exch})}$ of uptake (and of release and exchange) we may once again apply eq. (13), now however with a totally different understanding since the "body"

whose uptake is now considered is exclusively the space of micropores. For quantitating its "extension" R_2 we have to use eq. (15) in the form

$$R_2 = \frac{3(V_{\text{cryst.}} - V_1)}{A}, \tag{20}$$

where the difference between the crystal volume ($V_{\text{cryst.}}$) and mesopore volume (V_1) denotes the volume occupied by the micropores and A denotes the mutual interface between the two pore spaces. The diffusivity now appearing in eq. (13) is that within (exclusively!) the micropores, i.e. D_2.

Transport enhancement, i.e. the increase in the uptake (release, exchange) rate of the hierarchical adsorbent ($1/\tau$) in comparison with its purely microporous counterpart ($1/\tau_{\text{Diff}}$) of equal radius (R), is thus found to follow, in the two limiting cases, totally different dependencies, namely

$$\frac{1/\tau_{(\text{fast exch})}}{1/\tau_{\text{Diff}}} = \frac{p_1 D_1 + p_2 D_2}{D_2} \approx \frac{p_1 D_1}{D_2} \tag{21}$$

and

$$\frac{1/\tau_{(\text{slow exch})}}{1/\tau_{\text{Diff}}} = \frac{R^2}{R_2^2}. \tag{22}$$

The second relation in eq. (21) takes into account that significant transport enhancement in pore hierarchies necessitates the condition $p_1 D_1 \gg p_2 D_2$. With the notation of eq. (22) we have, furthermore, implied that the exchange between the micro- and mesopores is exclusively controlled by diffusion and not, additionally, affected by surface resistances. Following eqs. (13) and (14), with increasing miniaturization (i.e. by reducing the spherical particle size R [87]–[90]) transport inhibition by diffusion is found to decrease much more significantly than by surface permeation. Correspondingly, also with decreasing values of R_2, the influence of transport resistances at the interface between the space of micro- and mesopores becomes increasingly important. Attainment of the precondition of a diffusion-limited exchange between the micro- and mesopores becomes therefore increasingly questionable. Thus, it is in particular the advent of hierarchically porous materials, which makes a better understanding of transport resistances by surface barriers, to which we have referred already at the end of section 4, all the more urgent.

Since the overall phenomenon of uptake (tracer exchange, release) is dominated by the slower process, comparison of eqs. (21) and (22) provides us with a straightforward option to decide between the two limiting cases, attributing the condition

$$\frac{p_1 D_1}{D_2} \gg \frac{R^2}{R_2^2} \quad \text{to} \quad \text{slow exchange,} \tag{23}$$

$$\frac{p_1 D_1}{D_2} \ll \frac{R^2}{R_2^2} \quad \text{to} \quad \text{fast exchange.} \tag{24}$$

5.2 Diffusion in Pore Hierarchies by the Two-Region Model

The previous section has illustrated the potentials of Kinetic Monte Carlo simulations for elucidating the complexity of mass transfer in pore hierarchies. There are, in principle, no restrictions in the variety of pore architecture, which may be investigated in this way. It is true, however, that the technique itself sets narrow boundaries. Each pore space necessitates its particular treatment which, as a rule, has to be based on large data sets for an adequate description of the system under study.

In this context, an analytical treatment would offer much better prospects. Such a possibility is indeed provided by the two-region model of diffusion. Originally introduced for the analytical description of mass transfer in beds of nanoporous particles and, in particular, for its quantitation by PFG NMR [91],[92] it has, eventually, been applied quite generally for compartmented systems and, notably, for organic tissues [13],[93],[94]. Here it has been referred to as the Kärger model [95],[96]. Quite recently [97],[98] the formalism has also been applied to the description of mass transfer in hierarchically porous materials. It is based on a generalization of Fick's 2nd law by comprising mass transfer in both pore spaces, yielding

$$\frac{\partial c_1}{\partial t} = D_1 \frac{\partial^2 c_1}{\partial x^2} - \frac{1}{\tau_1} c_1 + \frac{1}{\tau_2} c_2 \tag{25}$$

$$\frac{\partial c_2}{\partial t} = D_2 \frac{\partial^2 c_2}{\partial x^2} - \frac{1}{\tau_2} c_2 + \frac{1}{\tau_1} c_1. \tag{26}$$

Concentrations (c_1 for meso-, c_2 for micropores) are defined with reference to unit volumes notably exceeding the size of the micro- and mesopores so that, within a given sample, they may be assumed to be of, essentially, identical topography [12]. Changes in local concentration (left terms in eqs. (25) and (26)) are caused by diffusion within the given pore system (first term on the right, corresponding to Fick's 2nd law) and departure from and arrival at the corresponding pore space (second and third term). Diffusivities D_i and mean lifetimes (τ_i) are assumed to be independent of concentration.

With eqs. (25) and (26), an entity of four parameters is found to suffice for the quantitation of mass transfer in a hierarchically organized pore system. Molecular mean lifetimes in the two pore spaces are correlated with their relative equilibrium populations by the detailed balance equation

$$\frac{p_1}{\tau_1} = \frac{p_2}{\tau_2}. \tag{27}$$

Description of mass transfer may therefore alternatively be based on the diffusivities in the two pore spaces (D_1 and D_2), the mean lifetime τ_2 in the micropores and the relative population p_1 of the mesopores under equilibrium. Furthermore, it holds (see the beginning of Sect. 5.1) $D_1 \gg D_2$ and $p_1 \ll p_2$ (which, due to $p_1 + p_2 = 1$, also means $p_1 \ll 1$). Under these conditions the overall mass transfer is only affected by D_2 and τ_2 and the product $p_1 D_1$, i.e. the "efficiency" of mass transfer in the transport pores.

With eqs. (25) and (26), transitions between the two pore spaces are implied to occur with the same probability at any time, i.e. independent of the diffusion path length covered by the molecule. Such an assumption is strictly correct in only the limiting case of strong transport resistances at the boundary (i.e. the mutual interface) between the two pore spaces. Quantitating molecular exchange with a mean exchange time, however, remains a reasonable approach also under diffusion limitation. It is then commonly referred to as the linear driving force (LDF) approximation [99] (see also section 6.2.3.9 of [3]).

Under the combined influence of micropore diffusion and interface permeation, within the formalism of the statistical moments (see e.g. [37],[38] or section 13.6.2 in [3]) the mean exchange time results as simply the sum of the exchange time for each individual resistances. Hence, in such a case, eqs. (13) and (14) must be summed, with the extension R_2 of the space of micropores resulting from eq. (20).

Within the formalism of the two-region model for one-dimensional diffusion, mass transfer in a hierarchically organized pore system may easily be considered to occur under the conditions of chemical reactions. Under the simplifying assumption of an irreversible monomolecular reaction A→B, with the conversion probabilities (reaction rates) coinciding in the micro- and mesopores ($k_1 = k_2 = k$) and with identical diffusivities of the two molecular species in either pore space ($D_{Ai} = D_{Bi} = D_i$), one has

$$\frac{\partial c_{A1}}{\partial t} = D_1 \frac{\partial^2 c_{A1}}{\partial x^2} - \frac{1}{\tau_1} c_{A1} + \frac{1}{\tau_2} c_{A2} - k c_{A1} \tag{28}$$

$$\frac{\partial c_{A2}}{\partial t} = D_2 \frac{\partial^2 c_{A2}}{\partial x^2} - \frac{1}{\tau_2} c_{A2} + \frac{1}{\tau_1} c_{A1} - k c_{A2} \tag{29}$$

$$\frac{\partial c_{B1}}{\partial t} = D_1 \frac{\partial^2 c_{B1}}{\partial x^2} - \frac{1}{\tau_1} c_{B1} + \frac{1}{\tau_2} c_{B2} + k c_{A1} \tag{30}$$

$$\frac{\partial c_{B2}}{\partial t} = D_2 \frac{\partial^2 c_{B2}}{\partial x^2} - \frac{1}{\tau_2} c_{B2} + \frac{1}{\tau_1} c_{B1} + k c_{A2}, \quad , \tag{31}$$

with c_{Ai} and c_{Bi} denoting the concentration of reactant (A) and product (B) molecules in transport pores (i=1) and micropores (i=2).

We may now easily go one step further than in Fig. 9 and consider the situation during molecular uptake in parallel with the occurrence of molecular conversion [98]. We imply that the molecules (of species A) are provided in excess, so that the concentration of reactant molecules A at the system's external surface is kept constant and the concentration of product molecules B close to the surface is zero. Eqs. (28) to (31) must therefore be solved with the initial and boundary conditions

$$c_{Ai}(x, t = 0) = c_{Bi}(x, t = 0) = 0, \quad 0 < x < L, \quad i = 1, 2 \tag{32}$$

$$c_{Ai}(x = 0, t) = c_{Ai}(x = L, t) = c_{Ai,eq} = \left(c_{A1,eq} + c_{A2,eq}\right) p_i, \quad 0 \le t < \infty, \quad i = 1, 2 \tag{33}$$

$$c_{Bi}(x = 0, t) = c_{Bi}(x = L, t) = 0, \quad 0 \le t < \infty, \quad i = 1, 2. \tag{34}$$

We are going to consider the special case that the molecular mean lifetime within the catalyst particle is of the order of the mean reaction time $1/k$ and that overall mass transfer occurs in one of the two limiting cases, i.e. under the condition of, respectively, slow and fast exchange between the two pore spaces.

Details of the calculations and a more extensive presentation of the data may be found in [98]. As a remarkable feature, the concentration profiles in the left of Fig. 10 are immediately seen to follow the pattern as observed already by KMC simulation (Fig. 9). This means constancy of concentration – now with both the reactant and product molecules - over the major part of the particle for slow exchange. Under fast exchange conditions, the reactant molecules are, once again, seen to penetrate the particle following a diffusion front. By closer inspection of the evolution of the profiles of the reactant and product molecules, their sum may easily be

anticipated to exactly follow what has been observed with Fig. 9 for molecular uptake without conversion.

On comparing the time dependence of the total amount of reactant and product molecules as shown on the right, increase in concentration of the reactant molecules is seen to occur at a much faster rate. This does not seem unreasonable since the entry of the reactant molecules precedes the formation of the product molecules. Finally, the total amounts of reactant and product molecules are seen to approach each other. This is the immediate consequence of having considered coinciding uptake and conversion rates.

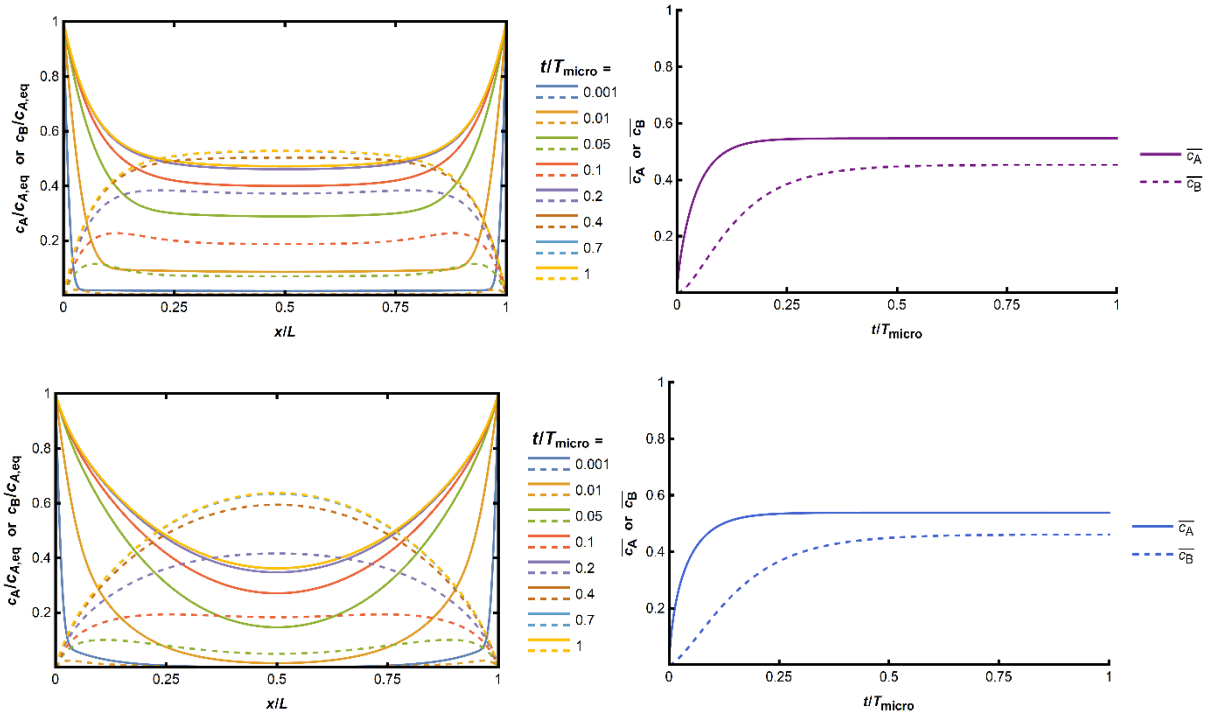

Figure 10: Transient concentration profiles (left) and relative uptake (right) of the reactant (full lines) and product (broken lines) molecules for coinciding uptake and conversion rates under the conditions of slow exchange (top; $\frac{1}{k} = \tau = \tau_{(\text{slow exch})} = 10 \times \tau_{(\text{fast exch})}$) and fast exchange (bottom; $\frac{1}{k} = \tau = \tau_{(\text{fast exch})} = 10 \times \tau_{(\text{slow exch})}$). Reproduced from [98].

5.3 Challenges of Diffusion Measurement in Pore Hierarchies

Already in the simplest case of purely microporous adsorbents, with the intracrystalline diffusivity as the only parameter of crucial relevance, experimental measurement of this single quantity proved to be a task that took decades [41],[100] and has not lost its relevance till this day [101],[102]. Elucidation of mass transfer in pore hierarchies must therefore be expected to be a by far more challenging task since it depends on a whole set of parameters rather than on a single quantity. The situation is additionally complicated by the fact that, for a given hierarchically organized material, these parameters are also a function of the molecules under study just as of their concentration and the given temperature. Finally, nanoporous materials are known to be highly susceptible to the treatment that they are subject to during synthesis, storage and application [103]. Therefore, in many cases, even the creation of reproducible conditions is a challenge on its own. It is therefore not surprising that a comprehensive experimental study of mass transfer focusing on all relevant parameters is still lacking and, as

a rule, no explicit specification has been made between the limiting cases of fast and slow exchange.

From the context, given for the explanation of the experimental procedures, it appears that so far most of the PFG NMR studies with mesoporous zeolites [104]–[106] were performed under conditions of fast exchange. Correspondingly, the recorded diffusivities were found to nicely result as the mean of the diffusivities in the micro- and mesopores as predicted by eq. (18). The uptake experiments reported in refs. [107],[108], however, seem to be performed under the conditions of slow exchange. Under these conditions, following eq. (22) transport enhancement scales with the square of the ratio between the particle size and the extension R_2 of the space of micropores. In such a situation, it makes indeed sense to follow a current custom and to rationalize transport enhancement in pore hierarchies with a reduction of the diffusion path length. Under fast exchange conditions, however, such a perspective might be misleading and it makes more sense to attribute transport enhancement to the creation of additional fast diffusion pathways.

In view of the distinct differences in transient concentration profiles during uptake (and release) as exemplified with Figs. 9 and 10, microimaging may be expected to be ideally suited for the in-depth study of mass transfer in hierarchically structured pore spaces. This type of material is, as a rule, permeated by a three-dimensional pore system. Therefore, preparation of particles with sealed, i.e. impermeable, top and bottom surfaces, as a prerequisite for the observation of profiles like those shown in Fig. 6, has proved to be a particular challenge. It is the focus of current research.

While the time window of microimaging starts with tens of seconds, PFG NMR is able to follow mass transfer from milliseconds up to (under particularly favorable conditions) seconds. With eq. (8), the signal attenuation of PFG NMR has been shown to be the Fourier transform of the mean propagator. For diffusion in pore hierarchies, the mean propagator results as the solution of eqs. (25) and (26) with the initial and boundary conditions

$$c_{i,norm}(x, t = 0) = p_i \delta(x) \tag{35}$$

and

$$c_{i,norm}(x = \pm\infty, t) = 0, \tag{36}$$

where we have used the normalized concentrations $c_{i,norm} = c_i/(c_{1,eq} + c_{2,eq})$. $\delta(x)$ denotes the Dirac delta function. Fourier transform of the solution finally yields [13],[92],[97],[109]

$$\psi(t) = \psi_1(t) + \psi_2(t) = p'_1 \exp(-q^2 D'_1 t) + p'_2 \exp(-q^2 D'_2 t) \tag{37}$$

with

$$D'_{1(2)} = \frac{1}{2}\left(D_1 + D_2 + \frac{1}{q^2}\left(\frac{1}{\tau_1} + \frac{1}{\tau_2}\right) \mp \left\{\left[D_2 - D_1 + \frac{1}{q^2}\left(\frac{1}{\tau_2} - \frac{1}{\tau_1}\right)\right]^2 + \frac{4}{q^2\tau_1\tau_2}\right\}^{\frac{1}{2}}\right), \tag{38}$$

$$p'_1 = 1 - p'_2, \quad p'_2 = \frac{1}{D'_2 - D'_1}(p_1 D_1 + p_2 D_2 - D'_1) \tag{39}$$

and

$$q = \gamma \delta g \tag{40}$$

as a measure of the gradient pulse intensity. PFG NMR signal attenuation (eq. (37)) is thus found to be the superposition of two attenuation curves for normal diffusion (eq. (9), with their diffusivities ($D'_{1(2)}$) and relative contributions ($p'_{1(2)}$) following (via eq. (38) and (39)) from the diffusivities in the two regions, their relative populations and the exchange rate between them. Under the condition $D_1 \gg D_2$ and $p_1 \ll p_2$ (in PFG NMR referred to as the third special case [91],[92],[109]), eqs. (37) – (39) are simplified to

$$\psi(q,t) = \exp\left[-q^2\left(D_2 + \frac{p_1 D_1}{q^2 \tau_2 p_1 D_1 + 1}\right)t\right]. \tag{41}$$

As an example of the output of such studies, Fig. 11a shows the PFG NMR attenuation curves due to diffusion of *n*-hexane in a granule of zeolite NaY. In the material under study (Figs. 11b and c), the continuous microporous phase is formed by an assemblage of zeolite crystallites, interconnected by zeolite bridges which have been generated in a secondary stage of crystallization [110],[111]. We note that the theoretical formalism, eq. (41), as resulting from the application of the two-region model to diffusion in mesoporous zeolites (lines in Fig. 11a), provides a reasonable prediction of the experimentally determined attenuation curves, allowing a first-order estimate of the key parameters ($p_1 D_1$, D_2 and τ_2) for mass transfer in such materials. Quantification of the reliability of their determination is one of the tasks of ongoing studies.

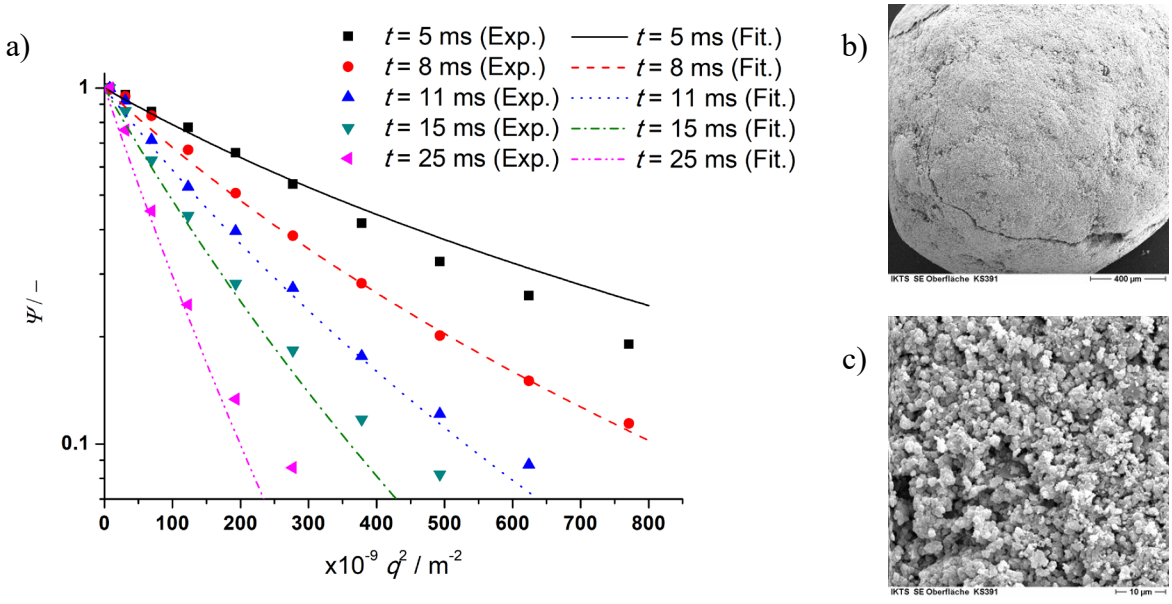

Figure 11: Transient PFG NMR attenuation curves for diffusion of *n*-hexane in binderless granules of zeolite NaY at room temperature (a) and microscans of a granule of the zeolite material (b) and its cross-section (c). The points are the experimental data (Exp.) and the lines are fitted curves (Fit.) of eq. (41) to the experimental attenuation curves, with $p_1 D_1 = 4 \times 10^{-10}$ m^{2}s^{-1}, $D_2 = 1.2 \times 10^{-10}$ m^{2}s^{-1} and $\tau_2 = 2$ ms. Reproduced from [97].

6. Conclusion

Fig. 1 served for an illustration of the various length scales to be covered by the molecules in industrial plants operating with nanoporous materials. We have, in the following, concentrated on presenting the particular challenges that one is confronted with on studying molecular diffusion within the interior of the individual particles as seen in the bottom of Fig. 1. Pulsed field gradient (PFG) NMR (under equilibrium conditions) and microimaging (by IR and interference microscopy, operating under non-equilibrium) have been shown to provide evidence on a wealth of phenomena. This evidence is, moreover, attained in a most direct way so that, in general, misinterpretations can be excluded. Like with any measuring techniques, however, there exist (sometimes even quite narrow) limits of their application. They include, in particular, the range of displacements, which are typically on the order of micrometers. Techniques that are sensitive to displacements of this order are commonly referred to as microscopic.

A comprehensive understanding of mass transfer necessitates, as a matter of course, knowledge about the rate of molecular transportation over all distances of relevance for overall performance. This includes the elementary steps of diffusion, such as the molecular jumps between the individual pores shown on the right of Fig. 1. Such measurements are called submicroscopic. Diffusion measurements with an individual crystal without the option to capture its interior are named mesoscopic. The resulting diffusivity is thus only an average over the transport properties of the given crystal. Macroscopic measurements operate with beds or pellets (as shown on the left of Fig. 1).

Tab. 1 provides a compilation of the most frequently used techniques of diffusion measurement in nanoporous materials. Distinction is made with reference to the diffusion path lengths typically considered in the measurements (ranging from submicroscopic till macroscopic) and between equilibrium and non-equilibrium measurement. As is common, the classification is not without some arbitrariness. Information about equilibrium properties, e.g., may as well be attained by non-equilibrium techniques, e.g. the self-diffusivity by tracer exchange. Vice versa, NMR measurements may be performed under both equilibrium and non-equilibrium.

Measurement	under Equilibrium	under Non-Equilibrium
Submicroscopic	Solid-State NMR [112],[113] Quasi-Elastic Neutron Scattering (QENS) [17]	
Microscopic	Pulsed Field Gradient (PFG) NMR [14],[114] Single-Particle Tracking (SPT) [19]	Microimaging [115]
Mesoscopic	Dynamic Light Scattering (DLS) [116]	(Single-Crystal)-Membrane Permeation [117]
Macroscopic		Adsorption/Desorption Kinetics [118] Liquid-Phase Batch Kinetics [101] Column Breakthrough Dynamics [119]

		Zero Length Columns (ZLC) Technique [120] Frequency Response (FR) Technique [121] NMR Imaging (MRI) [122] X-Ray Computed Tomography (XCT) [123]

Table 1: Classification of the various techniques of diffusion measurement with nanoporous host-guest systems with reference to the scale of observation ("Microscopic vs. Macroscopic") and the conditions, under which the measurements are (generally) performed ("Equilibrium vs. Non-Equilibrium"), after [124]

The references given in this table are the output of the first step within an IUPAC activity "to provide a first comprehensive set of guidelines for measurements and reporting of diffusion properties of chemical compounds in nanoporous materials serving for catalytic, mass separation and other relevant purposes" (Project Details - IUPAC | International Union of Pure and Applied Chemistry) [125]. We trust that also the present contribution will serve this goal.

Acknowledgement:

Financial support by the German Research Foundation is gratefully acknowledged. We highly appreciate the cooperation with many colleagues, both in our own affiliations at Leipzig University and the Saxon Academy of Sciences and Humanities and in many more institutions all over the world, and its promotion within the frame of an IUPAC activity dedicated to "Diffusion in Nanoporous Solids". We are obliged to the organizers of the DIMAT 2021 conference in Debrecen, Hungary, for the invitation to a talk, which served as a basis for this presentation.

References

[1] F. Schüth, K.S.W. Sing, J. Weitkamp (Eds.), Handbook of Porous Solids, Wiley-VCH, Weinheim, 2002.

[2] M. Thommes, K. Kaneko, A.V. Neimark, J.P. Olivier, F. Rodriguez-Reinoso, J. Rouquerol, and K.S. Sing, Physisorption of gases, with special reference to the evaluation of surface area and pore size distribution (IUPAC Technical Report), *Pure and Applied Chemistry* **87** (2015).

[3] J. Kärger, D.M. Ruthven, and D.N. Theodorou, Diffusion in Nanoporous Materials, Wiley - VCH, Weinheim, 2012.

[4] C. Baerlocher, McCusker, L. B., and D.H. Olson, Atlas of Zeolite Framework Types, Elsevier, Amsterdam, 2007.

[5] J. Weitkamp, Zeolites and Catalysis, *Solid State Ionics* **131** (2000) 175–188.

[6] M.A. Murphy, Early Industrial Roots of Green Chemistry, *Chemistry International* **43** (2021) 21–25.

[7] H. Mehrer, Diffusion in Solids, Springer, Berlin, 2007.

[8] J. Philibert, Atom Movement - Diffusion and Mass Transfer in Solids, Les Editions de Physique, Les Ulis, Cedex A, 1991.

[9] H. Schmalzried, Chemical Kinetics of Solids, Verlag Chemie, Weinheim, 1995.

[10] J. Kärger, C. Chmelik, and R. Valiullin, Die innere Größe macht's: Moleküldiffusion in nanoporösen Materialien, *Physik Journal* **12** (2013) 39–45.

[11] I. Prigogine, The End of Certainty, The Free Press, New York, London, Toronto, Sydney, 1997.

[12] T. Titze, A. Lauerer, L. Heinke, C. Chmelik, N.E.R. Zimmermann, F.J. Keil, D.M. Ruthven, and J. Kärger, Transport in Nanoporous Materials Including MOFs: The Applicability of Fick's Laws, *Angew. Chem. Int. Ed.* **54** (2015) 14580–14583.

[13] W.S. Price, NMR Studies of Translational Motion, University Press, Cambridge, 2009.

[14] J. Kärger, M. Avramovska, D. Freude, J. Haase, S. Hwang, and R. Valiullin, Pulsed field gradient NMR diffusion measurement in nanoporous materials, *Adsorption* **27** (2021) 453–484.

[15] H. Jobic, Investigation of Diffusion in Molecular Sieves by Neutron Scattering Techniques, in: H.G. Karge, J. Weitkamp (Eds.), Science and Technology - Molecular Sieves, vol. 7, Adsorption and Diffusion, Springer, Berlin, Heidelberg, 2008, pp. 207–233.

[16] H. Jobic, and D. Theodorou, Quasi-elastic neutron scattering and molecular dynamics simulations as complementary techniques for studying diffusion in zeolites, *Micropor. Mesopor. Mat.* **102** (2007) 21–50.

[17] M. Kruteva, Dynamics studied by Quasielastic Neutron Scattering (QENS), *Adsorption* **27** (2021) 875–889.

[18] C. Bräuchle, D.C. Lamb, J. Michaelis (Eds.), Single Particle Tracking and Single Molecule Energy Transfer, Wiley-VCH, Weinheim, 2010.

[19] J.J.E. Maris, D. Fu, F. Meirer, and B.M. Weckhuysen, Single-molecule observation of diffusion and catalysis in nanoporous solids, *Adsorption* **27** (2021) 423–452.

[20] J. Philibert, One and a Half Century of Diffusion: Fick, Einstein, before and beyond, in: J. Kärger, F. Grinberg, P. Heitjans (Eds.), Diffusion Fundamentals, Leipziger Universitätsverlag, Leipzig, 2005, pp. 8–17.

[21] H. Mehrer, and N.A. Stolwijk, Heroes and highlights in the history of diffusion, in: C. Chmelik, N.K. Kanellopoulos, J. Kärger, D. Theodorou (Eds.), Diffusion Fundamentals III, Leipziger Universitätsverlag, Leipzig, 2009, pp. 21–52.

[22] G.D. Birkhoff, Proof of the Ergodic Theorem, *Proc. Nat. Acad. Sci.* **17** (1931) 656–660.

[23] F. Feil, S. Naumov, J. Michaelis, R. Valiullin, D. Enke, J. Kärger, and C. Bräuchle, Single-particle and ensemble diffusivities - test of ergodicity, *Angew. Chem. Int. Ed.* **51** (2012) 1152–1155.

[24] A. Feldhoff, J. Caro, H. Jobic, C.B. Krause, P. Galvosas, and J. Kärger, Intracrystalline Transport Resistances in Nanoporous Zeolite X, *ChemPhysChem* **10** (2009) 2429–2433.

[25] C.P. Slichter, Principles of Magnetic Resonance, Springer, Berlin, 1980.

[26] R. Kimmich, NMR Tomography, Diffusometry, Relaxometry, Springer, Berlin, 1997.

[27] R. Valiullin, Diffusion NMR of Confined Systems, Royal Society of Chemistry, Cambridge, 2016.

[28] J. Kärger, Transport Phenomena in Nanoporous Materials, *ChemPhysChem* **16** (2015) 24–51.

[29] J. Kärger, and W. Heink, The Propagator Representation of Molecular Transport in Microporous Crystallites, *J. Magn. Reson.* **51** (1983) 1–7.

[30] P.T. Callaghan, A. Coy, D. MacGowan, K.J. Packer, and F.O. Zelaya, Diffraction-like effects in NMR diffusion studies of fluids in porous solids, *Nature* **351** (1991) 467–469.

[31] C. Chmelik, and J. Kärger, In-situ Study on Molecular Diffusion Phenomena in Nanoporous Catalytic Solids, *Chem. Soc. Rev.* **39** (2010) 4864–4884.

[32] J. Kärger, H. Pfeifer, E. Riedel, and H. Winkler, Self-diffusion measurements of water adsorbed in NaY zeolites by means of NMR pulsed field gradient techniques, *J. Coll. Interf. Sci.* **44** (1973) 187–188.

[33] J. Kärger, and P. Volkmer, Comparison of Predicted and Nuclear Magnetic Resonance Zeolitic Diffusion Coefficients, *J. Chem. Soc. Faraday Trans. I* **76** (1980) 1562–1568.

[34] F. D'Orazio, S. Bhattacharja, W.P. Halperin, and R. Gerhardt, Enhanced Self-Diffusion of Water in Restricted Geometry, *Phys. Rev. Lett.* **63** (1989) 43–46.

[35] D.M. Ruthven, Principles of Adsorption and Adsorption Processes, Wiley, New York, 1984.

[36] J. Kärger, A Study of Fast Tracer Desorption in Molecular Sieve Crystals, *AIche Journal* **28** (1982) 417–423.

[37] R.M. Barrer, Zeolites and Clay Minerals as Sorbents and Molecular Sieves, Academic Press, London, 1978.

[38] M. Kocirik, and A. Zikanova, The analysis of the adsorption kinetics in materials with polydisperse pore structure, *Ind. Eng. Chem. Fundamen.* **13** (1974) 347–350.

[39] J. Kärger, H. Pfeifer, F. Stallmach, M. Bülow, P. Struve, R. Entner, H. Spindler, and R. Seidel, Influence of Molecular Shape on Probing Mass-Transfer Resistances on Zeolites, *Aiche J.* **36** (1990) 1500–1504.

[40] J. Kärger, M. Bülow, B.R. Millward, and J.M. Thomas, A phenomenological Study of Surface Barriers in Zeolites, *Zeolites* **6** (1986) 146–150.

[41] J. Kärger, and S. Vasenkov, Quantitation of diffusion in zeolite catalysts, *Micropor. Mesopor. Mat.* **85** (2005) 195–206.

[42] J. Kärger, T. Binder, C. Chmelik, F. Hibbe, H. Krautscheid, R. Krishna, and J. Weitkamp, Microimaging of Transient Guest Profiles to Monitor Mass Transfer in Nanoporous Materials, *Nat. Mater.* **13** (2014) 333–343.

[43] U. Schemmert, J. Kärger, and J. Weitkamp, Interference Microscopy as a Technique for Directly Measuring Intracrystalline Transport Diffusion in Zeolites, *Micropor. Mesopor. Mat.* **32** (1999) 101–110.

[44] U. Schemmert, J. Kärger, C. Krause, R.A. Rakoczy, and J. Weitkamp, Monitoring the Evolution of Intracrystalline Concentration, *Europhys. Lett.* **46** (1999) 204–210.

[45] C. Chmelik, P. Kortunov, S. Vasenkov, and J. Kärger, Internal transport resistances and their influence on diffusion in zeolites as traced by microscopic measuring techniques, *Adsorption* **11** (2005) 455–460.

[46] C. Chmelik, L. Heinke, J.M. van Baten, and R. Krishna, Diffusion of n-butane/iso-butane mixtures in silicalite-1 investigated using infrared (IR) microscopy, *Micropor. Mesopor. Mat.* **125** (2009) 11–16.

[47] J. Crank, The Mathematics of Diffusion, Clarendon Press, Oxford, 1975.

[48] H.S. Carslaw, and J.C. Jaeger, Conduction of Heat in Solids, Oxford Science Publications, Oxford, 2004.

[49] P. Kortunov, L. Heinke, S. Vasenkov, C. Chmelik, D.B. Shah, J. Kärger, R.A. Rakoczy, Y. Traa, and J. Weitkamp, Internal Concentration Gradients of Guest Molecules in Nanoporous Host Materials: Measurement and Microscopic Analysis, *J. Phys. Chem. B* **110** (2006) 23821–23828.

[50] J. Kärger, and D.M. Ruthven, Diffusion in nanoporous materials: Fundamental principles, insights and challenges, *New J. Chem.* **40** (2016) 4027–4048.

[51] C. Chmelik, L. Heinke, P. Kortunov, J. Li, D. Olson, D. Tzoulaki, J. Weitkamp, and J. Kärger, Ensemble Measurement of Diffusion: Novel Beauty and Evidence, *ChemPhysChem* **10** (2009) 2623–2627.

[52] J. Cousin Saint Remi, A. Lauerer, C. Chmelik, I. Vandendael, H. Terryn, G.V. Baron, Denayer, Joeri F. M., and J. Kärger, The role of crystal diversity in understanding mass transfer in nanoporous materials, *Nat. Mater.* **15** (2015) 401–406.

[53] M. Stöcker, Methanol-to-Hydrocarbons: Catalytic Materials and Their Behavior [Review], *Micropor. Mesopor. Mat.* **29** (1999) 3–48.

[54] D.M. Ruthven, and S.C. Reyes, Adsorptive separation of light olefins from paraffins, *Micropor. Mesopor. Mat.* **104** (2007) 59–66.

[55] L. Heinke, P. Kortunov, D. Tzoulaki, and J. Kärger, The options of interference microscopy to explore the significance of intracrystalline diffusion and surface permeation for overall mass transfer on nanoporous materials, *Adsorption* **13** (2007) 215–223.

[56] L. Heinke, Significance of concentration-dependent intracrystalline diffusion and surface permeation for overall mass transfer, *Diffusion Fundam.* **4** (2007) 12.

[57] O.K. Dudko, A.M. Berezhkovskii, and G.H. Weiss, Diffusion in the presence of periodically spaced permeable membranes, *J. Chem. Phys.* **121** (2004) 11283–11288.

[58] O.K. Dudko, A.M. Berezhkovskii, and G.H. Weiss, Time-dependent diffusion coefficients in periodic porous materials, *J. Phys. Chem. B* **109** (2005) 21296–21299.

[59] D.M. Ruthven, J. Kärger, S. Brandani, and E. Mangano, Sorption kinetics: measurement of surface resistance, *Adsorption* **27** (2021) 787–799.

[60] J. Kärger, H. Pfeifer, R. Richter, H. Furtig, W. Roscher, and R. Seidel, NMR-Study of Mass-Transfer in Granulated Molecular-Sieves, *Aiche J.* **34** (1988) 1185–1189.

[61] J. Caro, M. Bülow, H. Jobic, J. Kärger, and B. Zibrowius, Molecular Mobility Measurement of Hydrocarbons in Zeolites by NMR Techniques, *Adv. Catal.* **39** (1993) 351–414.

[62] F. Hibbe, C. Chmelik, L. Heinke, S. Pramanik, J. Li, D.M. Ruthven, D. Tzoulaki, and J. Kärger, The Nature of Surface Barriers on Nanoporous Solids Explored by Microimaging of Transient Guest Distributions, *J. Am. Chem. Soc.* **133** (2011) 2804–2807.

[63] F. Hibbe, J. Caro, C. Chmelik, A. Huang, T. Kirchner, D. Ruthven, R. Valiullin, and J. Kärger, Monitoring Molecular Mass Transfer in Cation-Free Nanoporous Host-Crystals of Type AlPO-LTA, *J. Am. Chem. Soc.* **134** (2012) 7725–7732.

[64] N.E.R. Zimmermann, B. Smit, and F.J. Keil, On the Effects of the External Surface on the Equilibrium Transport in Zeolite Crystals, *J. Phys. Chem. C* **114** (2010) 300–310.

[65] N.E.R. Zimmermann, B. Smit, and F.J. Keil, Predicting Local Transport Coefficients at Solid–Gas Interfaces, *J. Phys. Chem. C* **116** (2012) 18878–18883.

[66] N.E.R. Zimmermann, T.J. Zabel, and F.J. Keil, Transport into Nanosheets: Diffusion Equations Put to Test, *J. Phys. Chem. C* **117** (2013) 7384–7390.

[67] A.F. Combariza, and G. Sastre, Influence of Zeolite Surface in the Sorption of Methane from Molecular Dynamics, *J. Phys. Chem. C* **115** (2011) 13751–13758.

[68] G. Sastre, J. Kärger, and D.M. Ruthven, Molecular Dynamics Study of Diffusion and Surface Permeation of Benzene in Silicalite, *J. Phys. Chem. C* **122** (2018) 7217–7225.

[69] M.W. Anderson, J.T. Gebbie-Rayet, A.R. Hill, N. Farida, M.P. Attfield, P. Cubillas, V.A. Blatov, D.M. Proserpio, D. Akporiaye, B. Arstad, and J.D. Gale, Predicting crystal growth via a unified kinetic three-dimensional partition model, *Nature* **544** (2017) 456–459.

[70] M. Suga, S. Asahina, Y. Sakuda, H. Kazumori, H. Nishiyama, T. Nokuo, V. Alfredsson, T. Kjellman, S.M. Stevens, H.S. Cho, M. Cho, L. Han, S. Che, M.W. Anderson, F. Schüth, H. Deng, O.M. Yaghi, Z. Liu, H.Y. Jeong, A. Stein, K. Sakamoto, R. Ryoo, and O. Terasaki, Recent progress in scanning electron microscopy for the characterization of fine structural details of nano materials, *Progress in Solid State Chemistry* **42** (2014) 1–21.

[71] L.R. Aramburo, L. Karwacki, P. Cubillas, S. Asahina, D.A.M. de Winter, M.R. Drury, I.L.C. Buurmans, E. Stavitski, D. Mores, M. Daturi, P. Bazin, P. Dumas, F. Thibault-Starzyk, J.A. Post, M.W. Anderson, O. Terasaki, and B.M. Weckhuysen, The porosity, acidity, and reactivity of dealuminated zeolite ZSM-5 at the single particle level: the influence of the zeolite architecture, *Chemistry* **17** (2011) 13773–13781.

[72] D. Kondrashova, A. Lauerer, D. Mehlhorn, H. Jobic, A. Feldhoff, M. Thommes, D. Chakraborty, C. Gommes, J. Zecevic, P. de Jongh, A. Bunde, J. Kärger, and R. Valiullin, Scale-dependent diffusion anisotropy in nanoporous silicon, *Sci. Rep.* **7** (2017) 40207.

[73] M. Hartmann, and W. Schwieger, Hierarchically-structured porous materials: from basic understanding to applications, *Chem. Soc. Rev.* **45** (2016) 3311–3312.

[74] W. Schwieger, A.G. Machoke, T. Weissenberger, A. Inayat, T. Selvam, M. Klumpp, and A. Inayat, Hierarchy concepts: classification and preparation strategies for zeolite containing materials with hierarchical porosity, *Chem. Soc. Rev.* **45** (2016) 3353–3376.

[75] A.G. Machoke, A.M. Beltrán, A. Inayat, B. Winter, T. Weissenberger, N. Kruse, R. Güttel, E. Spiecker, and W. Schwieger, Micro/macroporous system: MFI-type zeolite crystals with embedded macropores, *Adv. Mater. Weinheim* **27** (2015) 1066–1070.

[76] J. García-Martínez, K. Li (Eds.), Mesoporous Zeolites: Preparation, Characterization and Applications, Wiley-VCH, Weinheim, 2015.

[77] M. Choi, H.S. Cho, R. Srivastava, C. Venkatesan, D.H. Choi, and R. Ryoo, Amphiphilic organosilane-directed synthesis of crystalline zeolite with tunable mesoporosity, *Nature Mater.* **5** (2006) 718–723.

[78] J. Čejka, and S. Mintova, Perspectives of Micro/Mesoporous Composites in Catalysis, *Catalysis Reviews* **49** (2007) 457–509.

[79] J. Pérez-Ramírez, D. Verboekend, A. Bonilla, and S. Abelló, Zeolite Catalysts with Tunable Hierarchy Factor by Pore-Growth Moderators, *Adv. Funct. Mater.* **19** (2009) 3972–3979.

[80] J. García-Martínez, M. Johnson, J. Valla, K. Li, and J.Y. Ying, Mesostructured zeolite Y—high hydrothermal stability and superior FCC catalytic performance, *Catal. Sci. Technol.* **2** (2012) 987.

[81] S.M. Auerbach, N.J. Henson, A.K. Cheetham, and H.I. Metiu, Transport Theory For Cationic Zeolites - Diffusion of Benzene in Na-Y, *J. Phys. Chem.* **99** (1995) 10600–10608.

[82] S.M. Auerbach, Analytical Theory of Benzene Diffusion in Na-Y Zeolite, *J. Chem. Phys.* **106** (1997) 7810–7815.

[83] R. Krishna, and J.M. van Baten, Kinetic Monte Carlo Simulations of the loading dependence of diffusion in zeolites, *Chem. Eng. Technol.* **28** (2005) 160–167.

[84] A. Gupta, and R.Q. Snurr, A study of pore blockage in silicalite zeolite using free energy perturbation calculation, *J. Chem. Phys. B* **109** (2005) 1822–1833.

[85] S. Vasenkov, and J. Kärger, Evidence for the existence of intracrystalline transport barriers in MFI-type zeolites: a model consistency check using MC simulations, *Micropor. Mesopor. Mat.* **55** (2002) 139–145.

[86] D. Schneider, D. Kondrashova, R. Valiullin, A. Bunde, and J. Kärger, Mesopore-Promoted Transport in Microporous Materials, *Chem. Ingen. Techn.* **87** (2015) 1794–1809.

[87] S. Mintova, Mechanism of Zeolite A Nanocrystal Growth from Colloids at Room Temperature, *Science* **283** (1999) 958–960.

[88] M. Choi, K. Na, J. Kim, Y. Sakamoto, O. Terasaki, and R. Ryoo, Stable single-unit-cell nanosheets of zeolite MFI as active and long-lived catalysts, *Nature* **461** (2009) 246–249.

[89] P. Kumar, D.W. Kim, N. Rangnekar, H. Xu, E.O. Fetisov, S. Ghosh, H. Zhang, Q. Xiao, M. Shete, J.I. Siepmann, T. Dumitrica, B. McCool, M. Tsapatsis, and K.A. Mkhoyan, One-dimensional intergrowths in two-dimensional zeolite nanosheets and their effect on ultra-selective transport, *Nat. Mater.* **19** (2020) 443–449.

[90] J. Caro, and J. Kärger, From computer design to gas separation, *Nat. Mater.* **19** (2020) 374–375.

[91] J. Kärger, Zur Bestimmung der Diffusion in einem Zweibereichsystem mit Hilfe von gepulsten Feldgradienten, *Ann. Phys.* **24** (1969) 1–4.

[92] J. Kärger, Nmr Self-Diffusion Studies in Heterogeneous Systems, *Adv. Colloid Interface Sci.* **23** (1985) 129–148.

[93] A. Waldeck, P.W. Kuchel, A.J. Lennon, and B.E. Chapman, NMR diffusion measurements to characterise membrane transport and solute binding, *Progress in Nuclear Magnetic Resonance Spectroscopy* **30** (1997) 39–68.

[94] C.A. Clark, and D. Le Bihan, Water diffusion compartmentation and anisotropy at high b values in the human brain, *Magn. Reson. Med.* **44** (2000) 852–859.

[95] H. Haddar, J.R. Li, and S. Schiavi, Adapting the Kärger model to account for finite diffusion-encoding pulses in diffusion MRI, *IMA J Appl Math* **81** (2016) 779–794.

[96] W. Wang, F. Seno, I.M. Sokolov, A.V. Chechkin, and R. Metzler, Unexpected crossovers in correlated random-diffusivity processes, *New J. Phys.* **22** (2020) 83041.

[97] S. Hwang, J. Haase, E. Miersemann, and J. Kärger, Diffusion Analysis in Pore Hierarchies by the Two-Region Model, *Adv. Mater. Interfaces* **8** (2021) 2000749.

[98] S. Hwang, J. Kärger, and E. Miersemann, Diffusion and reaction in pore hierarchies by the two-region model, *Adsorption* **27** (2021) 761–776.

[99] E. Glueckauf, *Trans. Faraday Soc.* **51** (1955) 1540.

[100] J. Kärger, Measurement of diffusion in zeolites - A never ending challenge?, *Adsorption* **9** (2003) 29–35.

[101] S. Brandani, Kinetics of liquid phase batch adsorption experiments, *Adsorption* **27** (2021) 353–368.

[102] Wang, S. Brandani, and D.M. Ruthven, A review of common practices in gravimetric and volumetric adsorption kinetic experiments, *Adsorpt.-J. Int. Adsorpt. Soc.* (2021).

[103] J. Cejka, A. Corma, S. Zones (Eds.), Zeolites and Catalysis: Synthesis, Reactions and Applications, Wiley-VCH, Weinheim, 2010.

[104] D. Mehlhorn, R. Valiullin, J. Kärger, K. Cho, and R. Ryoo, Exploring the Hierarchy of Transport Phenomena in Hierarchical Pore Systems by NMR Diffusion Measurement, *Micropor. Mesopor. Mat.* **164** (2012) 273–279.

[105] D. Mehlhorn, R. Valiullin, J. Kärger, K. Cho, and R. Ryoo, Intracrystalline diffusion in mesoporous zeolites, *ChemPhysChem* **13** (2012) 1495–1499.

[106] D. Mehlhorn, A. Inayat, W. Schwieger, R. Valiullin, and J. Kärger, Probing mass transfer in mesoporous faujasite-type zeolite nanosheet assemblies, *ChemPhysChem* **15** (2014) 1681–1686.

[107] L. Gueudré, M. Milina, S. Mitchell, and J. Pérez-Ramírez, Superior Mass Transfer Properties of Technical Zeolite Bodies with Hierarchical Porosity, *Adv. Funct. Mater.* **24** (2014) 209–219.

[108] M. Rincon Bonilla, T. Titze, F. Schmidt, D. Mehlhorn, C. Chmelik, R. Valiullin, S.K. Bhatia, S. Kaskel, R. Ryoo, and J. Kärger, Diffusion Study by IR Micro-Imaging of Molecular Uptake and Release on Mesoporous Zeolites of Structure Type CHA and LTA, *Materials* **6** (2013) 2662–2688.

[109] J. Kärger, H. Pfeifer, and W. Heink, Principles and Application of Self-Diffusion Measurements by Nuclear Magnetic Resonance, *Advances in Magn. Reson.* **12** (1988) 2–89.

[110] K. Schumann, A. Brandt, B. Unger, and F. Scheffler, Bindemittelfreie zeolithische Molekularsiebe der Typen LTA und FAU, *Chemie Ingenieur Technik* **83** (2011) 2237–2243.

[111] K. Schumann, B. Unger, A. Brandt, and F. Scheffler, Investigation on the pore structure of binderless zeolite 13X shapes, *Micropor. Mesopor. Mat.* **154** (2012) 119–123.

[112] D.I. Kolokolov, D. Freude, and A.G. Stepanov, Dynamics in nanoporous materials probed by 2H solid state NMR: estimation of self-diffusion coefficients, *Adsorption* **27** (2021) 841–855.

[113] P. Selter, M.B. Schmithorst, and B.F. Chmelka, Hopping dynamics and diffusion of atoms, molecules, and ions in nanoporous solids by exchange NMR spectroscopy, *Adsorption* **27** (2021) 857–874.

[114] A. Baniani, S.J. Berens, M.P. Rivera, R.P. Lively, and S. Vasenkov, Potentials and challenges of high-field PFG NMR diffusion studies with sorbates in nanoporous media, *Adsorption* **27** (2021) 485–501.

[115] C. Chmelik, R. Gläser, J. Haase, S. Hwang, and J. Kärger, Application of microimaging to diffusion studies in nanoporous materials, *Adsorption* **27** (2021) 819–840.

[116] V. Beschieru, B. Rathke, and S. Will, Particle diffusion in porous media investigated by dynamic light scattering, *Micropor. Mesopor. Mat.* **125** (2009) 63–69.

[117] J. Caro, Diffusion coefficients in nanoporous solids derived from membrane permeation measurements, *Adsorption* **27** (2021) 283–293.

[118] J.-Y. Wang, E. Mangano, S. Brandani, and D.M. Ruthven, A review of common practices in gravimetric and volumetric adsorption kinetic experiments, *Adsorption* **27** (2021) 295–318.

[119] N.S. Wilkins, A. Rajendran, and S. Farooq, Dynamic column breakthrough experiments for measurement of adsorption equilibrium and kinetics, *Adsorption* **27** (2021) 397–422.

[120] S. Brandani, and E. Mangano, The zero length column technique to measure adsorption equilibrium and kinetics: lessons learnt from 30 years of experience, *Adsorption* **27** (2021) 319–351.

[121] Y. Wang, Identification of mass transfer resistances in microporous materials using frequency response methods, *Adsorption* **27** (2021) 369–395.

[122] A. Gupta, T. Stait-Gardner, and W.S. Price, NMR imaging and diffusion, *Adsorption* **27** (2021) 503–533.

[123] R. Pini, L. Joss, and S.A. Hosseinzadeh Hejazi, Quantitative imaging of gas adsorption equilibrium and dynamics by X-ray computed tomography, *Adsorption* **27** (2021) 801–818.

[124] R. Gläser, J. Kärger, and D.M. Ruthven, Diffusion in Nanoporous Solids in the Focus of IUPAC – A Tribute to Jens Weitkamp, *Chemie Ing. Techn.* **93** (2021) 893–901.

[125] J. Kärger, D.M. Ruthven, and R. Valiullin, Diffusion Research with Nanoporous Material: More Than Just a Random Walk?, *Chemistry International* **43** (2021) 25–29.